Cell Reports

Complex regulation of *Eomes* levels mediated through distinct functional features of the *Meteor* long non-coding RNA locus

Graphical abstract

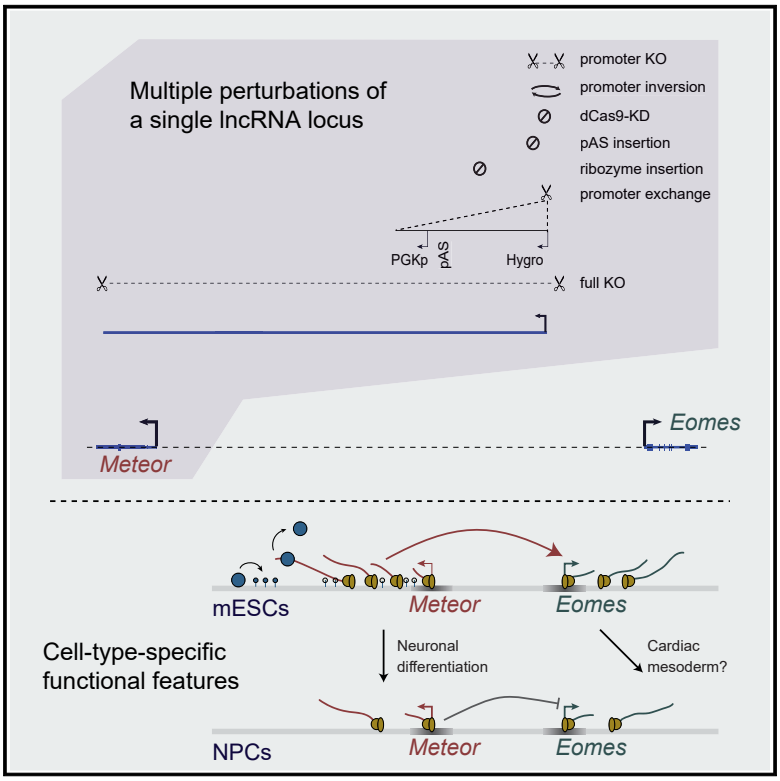

Highlights

- An array of perturbations targeting the *Meteor* long non-coding RNA locus
- Transcription elongation through *Meteor* is required for *Eomes* activation in mESCs
- *Meteor* is dispensable for the formation of beating cardiomyocytes
- *Meteor* promoter DNA is required for suppressing *Eomes* during neuronal differentiation

Authors

Noa Gil, Rotem Ben-Tov Perry, Zohar Mukamel, Alex Tuck, Marc Bühler, Igor Ulitsky

Correspondence

igor.ulitsky@weizmann.ac.il

In brief

Using a wide array of perturbation techniques, Gil et al. dissect the locus encoding the *Meteor* long non-coding RNA and show that distinct cell-type-specific functional features within the locus fine-tune the spatiotemporal expression patterns of the nearby gene *Eomes* in mouse embryonic stem cells and during differentiation.

Gil et al., 2023, Cell Reports *42*, 112569
June 27, 2023
https://doi.org/10.1016/j.celrep.2023.112569

Cell Reports

CellPress
OPEN ACCESS

Report

Complex regulation of *Eomes* levels mediated through distinct functional features of the *Meteor* long non-coding RNA locus

Noa Gil,[1,5] Rotem Ben-Tov Perry,[1] Zohar Mukamel,[2] Alex Tuck,[3,6] Marc Bühler,[3,4] and Igor Ulitsky[1,7,*]

[1]Department of Immunology and Regenerative Biology and Department of Molecular Neuroscience, Weizmann Institute of Science, Rehovot 76100, Israel

[2]Department of Molecular Genetics, Weizmann Institute of Science, Rehovot 76100, Israel

[3]Friedrich Miescher Institute for Biomedical Research, 4058 Basel, Switzerland

[4]University of Basel, Basel, Switzerland

[5]Present address: Friedrich Miescher Institute for Biomedical Research, 4058 Basel, Switzerland

[6]Present address: SOPHiA Genetics SA, La Pièce 12, 1180 Rolle, Switzerland

[7]Lead contact

*Correspondence: igor.ulitsky@weizmann.ac.il

https://doi.org/10.1016/j.celrep.2023.112569

SUMMARY

Long non-coding RNAs (lncRNAs) are implicated in a plethora of cellular processes, but an in-depth understanding of their functional features or their mechanisms of action is currently lacking. Here we study *Meteor*, a lncRNA transcribed near the gene encoding EOMES, a pleiotropic transcription factor implicated in various processes throughout development and in adult tissues. Using a wide array of perturbation techniques, we show that transcription elongation through the *Meteor* locus is required for *Eomes* activation in mouse embryonic stem cells, with *Meteor* repression linked to a change in the subpopulation primed to differentiate to the mesoderm lineage. We further demonstrate that a distinct functional feature of the locus—namely, the underlying DNA element—is required for suppressing *Eomes* expression following neuronal differentiation. Our results demonstrate the complex regulation that can be conferred by a single locus and emphasize the importance of careful selection of perturbation techniques when studying lncRNA loci.

INTRODUCTION

Long non-coding RNAs (lncRNAs) are RNA polymerase II transcription products emanating from thousands of loci in mammalian genomes.[1–3] Concomitantly with the rise in the number of annotated lncRNAs, they have been implicated in a wide array of cellular processes. In particular, multiple lncRNAs have been shown to contribute to fine-tuning of exit from pluripotency and developmental programs.[4,5]

A substantial number of lncRNAs are transcribed from regions with enhancer characteristics[6–8] and, accordingly, multiple studies suggested lncRNA contributions to enhancer functionality, for example through bridging enhancer-promoter chromatin loops,[9,10] recruiting activating proteins,[11] or affecting nuclear localization.[12] Such lncRNA loci can operate through the use of distinct functional features within the lncRNA gene, with the functionality of most such lncRNAs apparently relying not on the mature RNA product but rather on the underlying DNA element or various aspects of the transcriptional process,[13–15] consistent with the generally poor conservation of these loci.[8,16]

The study of enhancer-transcribed lncRNAs is proving to be particularly challenging, as the reciprocal interactions and interdependencies between transcription, chromatin modifications, chromatin architecture, and nuclear localization complicate efforts to separate direct and indirect effects of lncRNA activity. Crucially, these processes vary in their sensitivity to both the on-target and side effects of different perturbation techniques. This is exemplified by the sometimes contradictory effects noted when using different perturbation techniques to study particular loci,[17,18] emphasizing the need to interpret the consequences of lncRNA perturbations with great care.

One enhancer-transcribed lncRNA of substantial interest is *Meteor*, also known as *Platr11*, *Gm26975*, or *linc1405*.[5,19,20] *Meteor* is transcribed from the *MesEndoderm Transcriptional Enhancer Organizing Region*, located ~70 kb downstream of the gene encoding the EOMES transcription factor (TF).[14,20] EOMES, also known as TBR2, is a member of the T-box family of TFs, and is a master regulator of many developmental processes.[21,22] *Eomes* is first expressed in the trophectoderm lineage, where it is required for self-renewal and early differentiation of trophoblast stem cells, so that *Eomes*-null embryos arrest shortly after implantation.[23–25] Within the inner cell mass, *Eomes* expression initially marks the region that will become the primitive streak, making it one of the earliest markers of gastrulation onset. While *Eomes* is downregulated prior to the end of gastrulation, it is again detected in the developing forebrain,[26,27] and has been attributed functions in various neuronal cell types both during development and in the adult brain[21,28] as well as

in several types of immune cells.[29–31] Owing to its involvement in and regulation of these eclectic developmental processes, *Eomes* expression levels and domains are themselves subject to tight regulation through *cis*-regulatory elements, some of which have been characterized.[32]

As befits its initial identification as a pluripotency-associated transcript,[5,19] *Meteor* expression is highly associated with the pluripotent state,[14,20] although one study indicated that its expression is upregulated in the embryonic heart and in mouse embryonic stem cell (mESC)-derived mesoderm precursors.[33] *Meteor*'s function is also subject to conflicting evidence. Two studies found that *Meteor* knockout (KO) caused reduction in *Eomes* expression in mESCs,[14,34] suggesting that *Eomes* is the direct target of the *Meteor* locus. In contrast, another study, using a similar deletion scheme (Figure S1A), did not note any effect on *Eomes* expression in mESCs, but rather changes in expression of other genes, possibly indicating an *Eomes*-independent function of the *Meteor* locus.[20] Nonetheless, all three studies agree that in mESCs, targeting of *Meteor*'s transcription or RNA product does not have any noticeable effects on *Eomes* expression or otherwise,[14,20,34] pointing to an RNA-independent function of the *Meteor* locus. In contrast, two additional studies argue in favor of an RNA-dependent *Meteor* function, showing that *Meteor* repression by either insertion of an early polyadenylation site (pAS)[20,33] or short hairpin RNAs (shRNAs)[33] caused significant reduction in the ability of mESCs to differentiate to functional cardiac mesoderm, though with conflicting evidence as to whether or not *Eomes* expression was the mediator of this activity. Specifically, one report suggested that during the process of cardiac mesoderm differentiation, *Meteor* functions in *trans*, as overexpression of one of the *Meteor* exons could rescue the phenotype of *Meteor* repression.[33] The reduced ability to differentiate to cardiac mesoderm was suggested to prime the mESCs to differentiate to the ectoderm lineage, exemplified by increased efficiency of neuronal differentiation.[20]

In this study, we set out to address some of the key unanswered questions regarding *Meteor* biology. What is the effect of *Meteor* repression in mESCs, and to what extent is it mediated through *Eomes*? What is the role of the *Meteor* locus in priming cardiac mesoderm differentiation, and what is the contribution of the lncRNA to this activity? What are the roles, if any, of the *Meteor* locus during neurogenesis? Finally, what is the functional feature within *Meteor* that carries out these activities? We use a variety of perturbation techniques to show that two distinct functional features within the *Meteor* locus—transcriptional elongation through the *Meteor* locus, and the underlying DNA element—modulate *Eomes* expression levels in opposing manners in distinct cellular states, illustrating the complexity of the roles played by lncRNA loci within gene-regulatory networks.

RESULTS

A suite of perturbation methods for interrogating the *Meteor* locus

To probe *Meteor* functionality and identify its functional features, we employed a suite of methods for perturbation of the *Meteor* locus in mESCs (Figures 1A and S1A–S1D). First, we used CRISPR-Cas9 and a pair of guide RNAs (gRNAs) targeted to the two sides of the *Meteor* transcription start site (TSS). This generated clones with homozygous KO of the *Meteor* promoter (pKO) that resulted in complete ablation of *Meteor* expression, and a clone with a homozygous inversion of the promoter (pInv) that showed very low and inefficient transcription to the other side of the *Meteor* promoter (Figures 1A–1C). The deletion/inversion encompassed ~550 bp, a more targeted region than the 1- to 3-kb region deleted in previous *Meteor* KO models (Figure S1A).[14,20] We also received cell lines in which the entire *Meteor* locus was removed (full KO, or fKO lines)[34] (Figure 1A). As a complementary approach that targets *Meteor* transcription without changing the DNA sequence, we infected vectors expressing gRNAs targeting the *Meteor* TSS into mESCs stably expressing a catalytically dead Cas9 (dCas9) protein (dCas9-KD [knockdown]),[35] which reduced *Meteor* levels by ~90% (Figure 1B). In addition, we generated cell lines which introduced a polyadenylation site (pAS) into the first intron of *Meteor* so as to reduce transcription through the *Meteor* locus, and similarly employed a cell line in which *Meteor* expression was destabilized by insertion of a self-cleaving ribozyme (Rz) sequence in its second exon[34] (Rz-KD, Figure 1A). Lastly, to separate the effects of locus transcription from the DNA sequence at the promoter, we generated promoter exchange (pEX) cell lines in which the constitutive PGK promoter was knocked in downstream of the *Meteor* promoter, so that the transcription from the *Meteor* promoter is blocked by a pAS and the *Meteor* region is transcribed from the PGK promoter instead (Figure 1A).

Transcription into the *Meteor* gene body enhances *Eomes* expression in mESCs

As previously noted,[14,34] KO of either the entire *Meteor* gene body (fKO) or only the promoter region (pKO) caused a significant reduction of ~50% in *Eomes* levels (Figures 1C and 1D). However, it is noteworthy that here and throughout, we saw a wide variability in both *Meteor* and *Eomes* expression levels among wild type (WT) and (in the case of *Eomes*) *Meteor* KO clones, especially when the cells were grown in serum, as can also be noted from the expression levels of these genes in the ESpresso single-cell RNA-sequencing (scRNA-seq) dataset (Figure S1E). This hindered our ability to detect a significant change in *Eomes* levels when assayed by qRT-PCR, which might explain contradicting previous reports.[20] While alkaline phosphatase staining confirmed that the *Meteor* pKO lines were pluripotent (Figure S1F), we suspected that even small changes in pluripotency state could affect expression of these genes and therefore cultured the cells in serum-free medium supplemented with PD0325901 and CHIR99021, selective inhibitors of MEK and GSK3 ("2i" medium). 2i conditions shield the cells from differentiation signals, resulting in a morphologically and transcriptionally uniform "ground state" of pluripotency,[36,37] which indeed resulted in more uniform reduction in *Eomes* expression upon *Meteor* KO (Figures 1C and 1D). This effect of *Meteor* on *Eomes* expression appears to be specific to the naive state of pluripotency, as *Meteor* pKO cells cultured in the presence of fibroblast growth factor and activin, conditions which favor the generation of a "primed" epiblast stem cell-like state, did not exhibit changes in *Eomes* levels (Figure 1E). These cells are

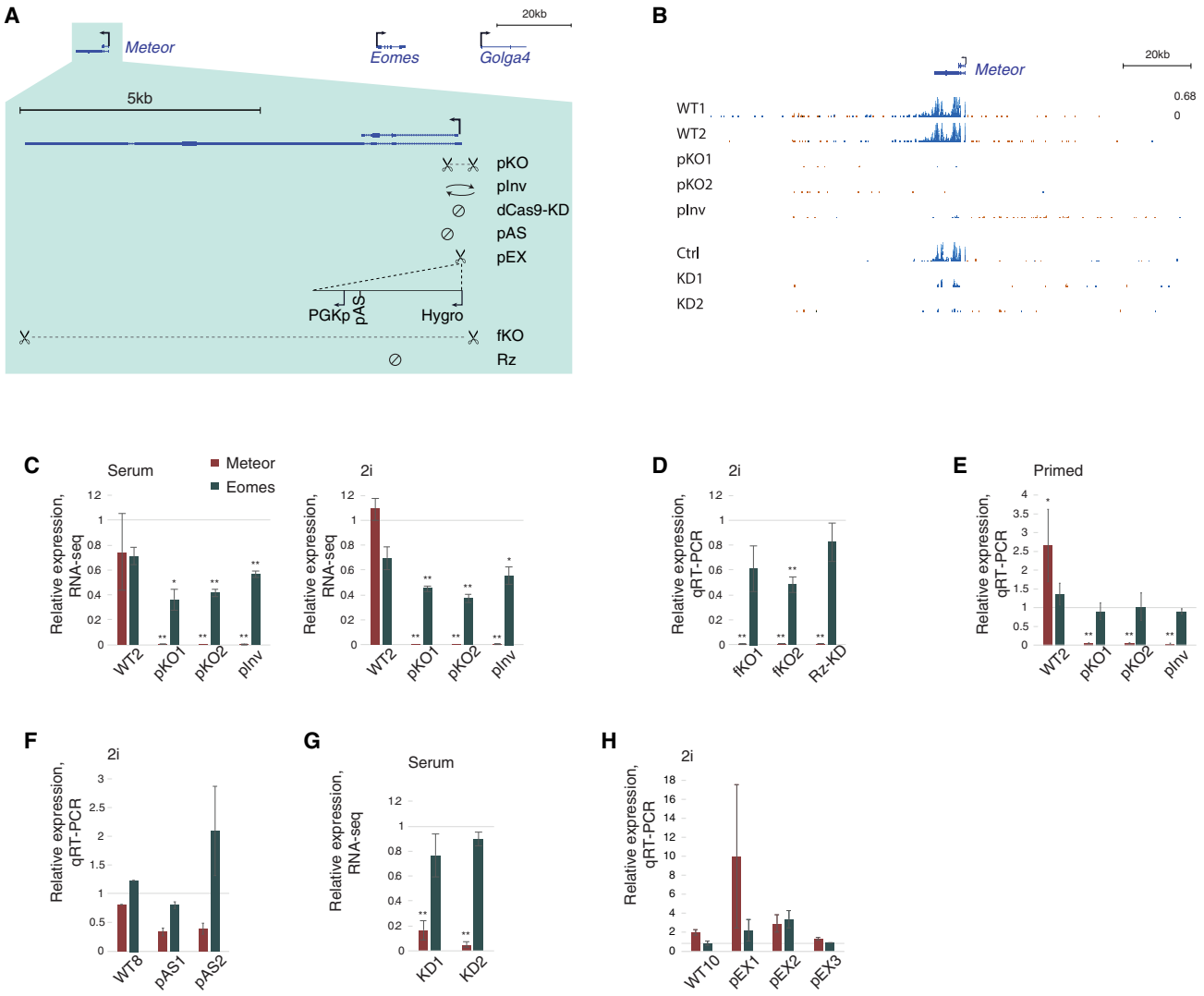

Figure 1. *Meteor* transcriptional elongation promotes *Eomes* expression in naive mESCs

(A) Perturbations used to analyze the *Meteor* locus in this study. Shown are the locations of gRNAs used for deleting or inverting the *Meteor* promoter (pKO) or gene body (fKO) or for inhibiting transcription (dCas9-KD); the locations of insertion of ribozyme (Rz) or polyadenylation (pAS) sequences; and the scheme for knocking in the PGK promoter downstream of the *Meteor* promoter (pEX). The fKO and Rz-KD mESC lines are the same as in Tuck et al.[34]

(B) RNA-seq tracks showing *Meteor* expression in the various pKO and pInv lines (grown in serum-free 2i/LIF conditions) and dCas9-KD lines (serum/LIF conditions). All tracks are normalized to the same scale. Orange denotes transcription on the plus strand, and blue denotes transcription on the minus strand.

(C) RNA-seq quantifications of *Meteor* and *Eomes* in *Meteor* pKO and pInv cell lines grown in serum/LIF (left) or serum-free 2i/LIF (right) conditions. Amounts normalized to WT1. Bars represent standard errors; n = 3. *p < 0.05, **p < 0.005.

(D) qRT-PCR quantifications of *Meteor* and *Eomes* levels in *Meteor* fKO and Rz-KD mESCs grown in serum-free 2i/LIF conditions. Levels were normalized to WT4 and *Ppib* for internal control. Bars represent standard errors; n = 8. *p < 0.05, **p < 0.005.

(E) Same as (D), for *Meteor* pKO and pInv mESCs grown in primed conditions, normalized to WT1. n = 4.

(F) Same as (D), for pAS clones grown in serum-free 2i/LIF conditions. Levels were normalized to WT7. n = 3.

(G) Same as (C), for *Meteor* dCas9-KD lines grown in serum/LIF conditions. Amounts normalized to Ctrl. n = 3. The dCas9-KD efficiencies of *Meteor* were 85% and 94% for KD1 and KD2, respectively.

(H) Same as (D), for pEX clones grown in serum-free 2i/LIF conditions. Levels were normalized to WT9. n = 3.

See also Figure S1.

found at a more advanced state of differentiation representative of the post-implantation embryo, in which lineage-specific markers, including *Eomes*, are induced compared with naive mESCs.[38,39] The lack of effect of *Meteor* repression on *Eomes* levels in primed cells suggests that *Eomes* induction at the onset of differentiation is not directly dependent on *Meteor* but rather is likely a consequence of altered cell state at the naive mESC stage (see below).

We were not successful in achieving substantial silencing of *Meteor* RNA levels using infections of shRNA-expressing

vectors, possibly due to the strong chromatin association of *Meteor* lncRNA (Figure S1G). Nonetheless, no significant changes in *Eomes* expression were noted when *Meteor* expression became undetectable through Rz-KD (Figure 1D), nor when a partially effective pAS was inserted into the first intron of *Meteor* (Figure 1F), suggesting that the *Meteor* RNA product likely does not contribute to *Eomes* regulation in mESCs. Furthermore, *Eomes* expression was not substantially affected when *Meteor* transcription was reduced by 80%–90% using dCas9-KD (Figure 1G). Interestingly, however, inversion of the *Meteor* promoter caused significantly reduced expression of *Eomes*, albeit to a slightly lower extent than the pKO (Figure 1C). As transcription from the *Meteor* promoter is initiated in this cell line, with evidence for inefficient elongation to the opposite direction (Figure 1B), this could indicate that transcription elongation into the *Meteor* locus—and specifically, the minimal level of elongation that still occurs in the *Meteor* dCas9-KD cells—is required for proper *Eomes* regulation in mESCs. Alternatively, the functional feature of the *Meteor* enhancer could be the underlying DNA sequence, which is left intact in the Rz-KD, pAS, and dCas9-KD cells lines, with the promoter inversion interfering with proper functionality of this DNA, for example by disrupting the integrity, arrangement, or orientation of TF binding sites (TFBSs). To examine this possibility, we used the JASPAR database[40] and FIMO[41] to systematically compare the predicted TFBSs in the WT and the inverted sequence. While only few differences were identified (Figure S1H), we cannot exclude the possibility that disruption of binding of one of these TFs plays a role in regulation of *Eomes* levels. Replacing the *Meteor* promoter with another constitutively expressed promoter increased expression of *Meteor*, albeit with a variable effect between different clones, but had no consistent effect on *Eomes* levels (Figure 1H). Combined, results from these various cell lines and perturbations suggest that the functional feature of the *Meteor* locus in mESCs is minimal transcription initiation or elongation into the *Meteor* gene body.

Reduced *Eomes* expression is associated with altered chromatin organization in mESCs

As *Meteor* is transcribed from an enhancer,[20] we next wanted to examine whether *Meteor* perturbations that are associated with *Eomes* downregulation are also manifested in an altered chromatin organization of the locus. We therefore probed the topology of the *Meteor* locus using targeted chromosome conformation capture (4C)[42] and CCCTC-binding factor (CTCF) chromatin immunoprecipitation sequencing (ChIP-seq). 4C analysis using either the *Meteor* or *Eomes* promoters as bait demonstrated spatial proximity between their respective loci, as has been shown previously[14]; deletion of either the entire *Meteor* gene body or the promoter region resulted in reduced contacts between the region surrounding *Meteor* and the *Eomes* locus, as did inversion of the *Meteor* promoter (Figures 2A, S2A, and S2B). In accordance with their lack of effect on *Eomes* levels, no significant changes between the *Meteor* and *Eomes* loci were noted in the dCas9-KD or Rz-KD mESC lines (Figures S2A and S2C).

These altered contacts between the *Eomes* and *Meteor* loci were not associated with any evident differential CTCF occupancy in the region (Figure 2A). It was shown that in mESCs, PRC2, the chromatin remodeler responsible for H3K27me3 deposition, modulates chromatin interactions between poised enhancers and their targets, thus promoting a chromatin topology required for proper induction of the target genes throughout differentiation processes.[44–46] Indeed, while the *Meteor* promoter region is associated with active chromatin, the region downstream to the *Meteor* gene body displays chromatin marks associated with both active (H3K27ac) and repressive (H3K27me3) states (Figure S2D). We therefore employed Cut&Run to map H3K27me3 deposition around the *Meteor* locus in mESCs carrying various *Meteor* perturbations. We noted an increase in H3K27me3 levels surrounding *Meteor* and its downstream enhancer region in the *Meteor* pKO lines (Figures 2B and S2E). These increased H3K27me3 levels upon *Meteor* repression would suggest that *Meteor* acts in preventing, rather than promoting, PRC2 recruitment and H3K27me3 deposition, in line with some indications that the binding of PRC2 to DNA and RNA is mutually antagonistic.[47–50] Accordingly, analysis of previously published PRC2 RNA immunoprecipitation (RIP) data[43] revealed that *Meteor* is within the top 5% of transcripts bound by EZH2, the catalytic subunit of PRC2 (Figure 2C), with data from an independent mESC RIP experiment[51] confirming an above-background association between *Meteor* and EZH2 but not with SUZ12, another PRC2 subunit (Figure S2F). The increased H3K27me3 deposition was also noted when the *Meteor* promoter was inverted (Figure 2B), altogether supporting a negative correlation between H3K27me3 deposition at the *Meteor* locus and *Eomes* expression in mESCs (Figures 1B and 2B). Combined, these results suggest that transcription through the *Meteor* gene body is required for restricting the spread of H3K27me3 in the *Meteor* enhancer region and enabling proper expression of *Eomes* in naive mESCs, with the nascent RNA likely mediating this function during its transcription while being dispensable after its production (see discussion).

Meteor repression does not alter the cardiac mesoderm differentiation potential of mESCs

We next wanted to examine the effects of *Meteor* transcription on the cardiac mesoderm differential potential of mESCs. To this end, we utilized the hanging-drop embryoid body (EB) differentiation system.[52] Consistent with its pluripotency-specific expression and with one previous study,[20] *Meteor* expression was quickly reduced in the early days of the EB differentiation protocol (Figure S3A). Markers for the three germ layers were induced throughout the differentiation, with a relatively low induction of ectoderm markers such as *Pax6* and *Otx2*, consistent with reduced efficiency of differentiation to the ectodermal lineage previously reported in this system for differentiation in leukemia inhibitory factor (LIF)-free and retinoic acid-free medium (Figure S3B).[53–55] Expression of *Eomes*, as well as additional early mesoderm markers such as *T* (Brachyury) and *FoxA2*, peaked at day 4 (Figure S3B).

Using qRT-PCR and RNA-seq, we monitored the effect of *Meteor* repression on mesodermal gene induction and cardiac mesoderm formation in this differentiation system. Perturbation of *Meteor* expression by either KO of its promoter or dCas9-KD did not lead to any significant reduction in the formation of

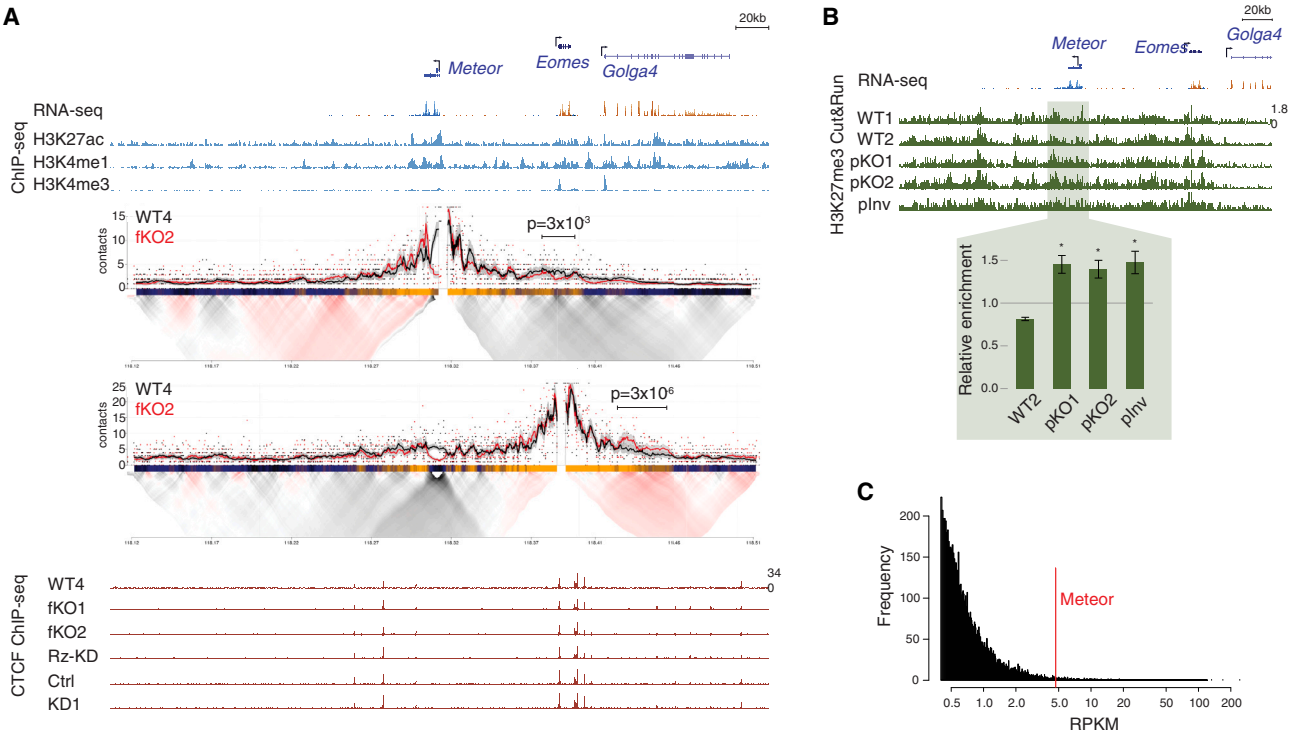

Figure 2. *Meteor* depletion induces chromatin changes in mESCs

(A) (Top) Genome browser image of the region surrounding the *Meteor* locus. Shown are representative transcript models; RNA-seq tracks where orange denotes transcription on the plus strand and blue denotes transcription on the minus strand; and ENCODE mESC ChIP-seq tracks. (Middle) 4C analysis in the indicated mESC lines using the *Meteor* or *Eomes* promoters as viewpoints. Domainograms showing mean contact per fragment end for a series of window sizes are placed below smoothed trend lines and raw counts of the contact profiles. (Bottom) ChIP-seq tracks of CTCF in the indicated mESC lines. All tracks are normalized to the same scale.

(B) (Top) Genome browser image of the region surrounding the *Meteor* locus. RNA-seq track is the same as shown in (A); Cut&Run analysis of H3K27me3 levels in the indicated mESC lines grown in serum-free 2i/LIF conditions. (Bottom) Bar plot shows quantification of signal in the highlighted region, normalized to WT1 and to a H3K27me3-rich region near the *Ppib* gene (see STAR Methods). Bars represent standard errors; n = 3. *p < 0.05, one-sided t test.

(C) Distribution of reads per kilobase per million (RPKM) of all transcripts identified in an EZH2 RNA immunoprecipitation (RIP) dataset taken from Zhao et al.[43] RPKM of *Meteor* indicated by a red line.

See also Figure S2.

beating foci in EBs at either day 9 or day 12 (Figures 3A and 3B). This is in stark contrast to previous reports in which *Meteor* repression led to severe inhibition of functional cardiac mesoderm, with only 0%–20% of EBs exhibiting beating foci.[20,33] Accordingly, and likewise in contrast to previous reports, we did not note any consistent changes in expression of *Eomes* or other mesodermal marker genes in either the pKO or dCas9-KD cells throughout the differentiation process (Figures 3C, S3C, and S3D). Specifically, no decrease in *Eomes* expression was noted at day 4, which is the peak of *Eomes* induction during differentiation of WT cells.

This deviation from previous reports might suggest that *Meteor* regulation of *Eomes* throughout EB differentiation depends on the genetic background of the mESCs. However, we could not find any consistent effect on either the levels or timing of activation of *Eomes* or additional mesoderm marker genes in mESCs derived from another background (129-C57Bl/6 mESCs), in which the full *Meteor* gene body was removed (fKO) or *Meteor* RNA was destabilized by insertion of a self-cleaving ribozyme sequence (Rz-KD)[34] (Figures 1A and S3E). Nevertheless, we cannot rule out that accumulated genomic or karyotypic aberrations in our cell lines affect their pluripotency status or differentiation potential, a general concern with long-term culture of pluripotent stem cells in general and those undergoing clonal selection in particular.[56,57]

The most likely explanation for the inconsistency with previous reports stems from the difference in the growth medium in which the mESCs were kept prior to onset of the differentiation. Specifically, while in previous reports the mESCs were cultured in serum-based medium,[20,33] we cultured the cells in 2i medium pre-differentiation. mESCs grown in either serum or 2i conditions are considered to be found in a "naive" state of pluripotency and retain the ability to differentiate into the three germ layers, although both protocols are associated with some alterations to differentiation potential. Specifically, serum-cultured cells exhibit high transcriptomic variability, with a subset of the population found at a more differentiated state with elevated expression of lineage-determination genes.[36,37,58,59] Therefore, and given the discrepancy in cardiac mesoderm differentiation when *Meteor* is depleted despite similar effects on *Eomes* levels

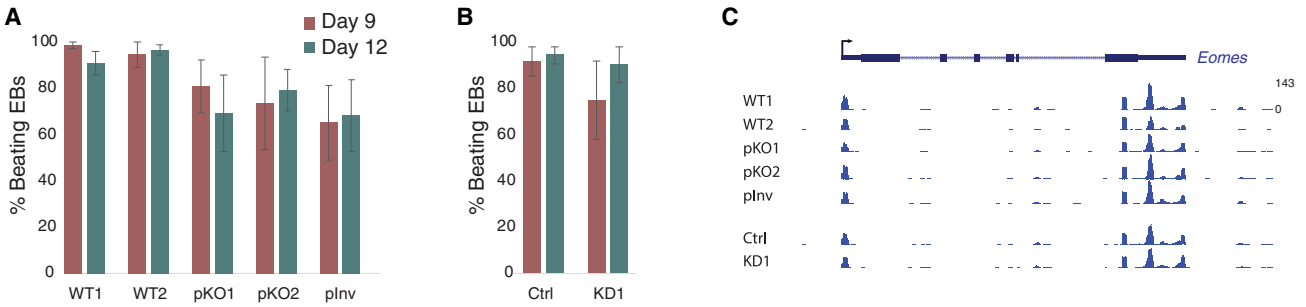

Figure 3. Embryoid body differentiation of *Meteor*-depleted cells

(A) Percentage of EBs that have beating foci at day 9 and day 12 of EB differentiation in the indicated cell lines. Bars represent standard errors; n = 3.

(B) Same as (A), for *Meteor* dCas9-KD cells.

(C) 3′ RNA-seq tracks of the *Eomes* locus on day 4 of EB differentiation in the indicated cell lines. All tracks are normalized to the same scale.

See also Figure S3.

in mESCs, we reasoned that *Meteor* repression affects cardiac mesoderm differentiation indirectly through affecting the cellular state at the naive mESC stage, an effect that is particularly apparent when mESCs are cultured in serum.

Meteor and *Eomes* are expressed in distinct mESC subpopulations

To test this hypothesis, we performed scRNA-seq to characterize the effect of *Meteor* KO on *Eomes* expression and cellular state in serum-grown mESCs. Approximately 750 cells from either one WT or one *Meteor* pKO line were assayed. scRNA-seq data showed that both *Meteor* and *Eomes* are variably expressed in mESCs, with *Meteor* detected ($\geq$1 reads) in just ~9% of the WT cells (Figure S4A). About a quarter of WT cells had detectable expression of *Eomes*, mostly at low levels of 1–4 reads/cell, although a small population (~2.5% of all cells) expressed *Eomes* at higher levels (Figure S4A).

We analyzed the scRNA-seq data using the MetaCell package,[60] which partitions the cells into groups of metacells (MCs) that represent a single putative cellular state. Interestingly, despite their spatial proximity and the regulatory link offered by the reduced expression of *Eomes* in *Meteor* KO cells (Figure 1C), *Meteor* and *Eomes* were predominantly expressed in non-overlapping MCs (Figures 4A, 4B, S4B, and S4C) ($p = 0.046$; one-sided Fisher's test considering only WT cells). *Eomes* was enriched primarily in MCs that express genes associated with a more differentiated state, such as *T*, *Lhx1*, and *Otx2*.[61–63] Accordingly, gene ontology (GO) term analysis of the top 100 genes correlated with *Eomes* expression in this dataset yielded terms such as "anterior/posterior axis specification" and "gastrulation" (Figure S4D). *Meteor*, on the other hand, was enriched in a subset of MCs that are associated with high expression of pluripotency genes, such as *Esrrb* and *Sox2* (Figures 4B, S4B, and S4C).

Altered expression of pluripotency-associated programs of *Meteor*-depleted mESCs

scRNA-seq was performed in parallel on *Meteor* WT and pKO cells. The total number of cells occupying MCs associated with high levels of pluripotency markers (MCs 5–15; Figures 4B, S4B, and S4C) was similar in the WT and pKO line (Figure S4E). However, among those MCs, there was a shift of pKO cells from MCs 6–8 to MCs 12–14 (Figures 4C and S4E). Examination of the genes differentially expressed between these MC groups indicates that MCs 12–14, which are more dominant in the *Meteor* pKO cells, preferentially expressed pluripotency-related and primordial germ cell-related genes such as *Dppa3*, *Zbtb10*, and *Nanos3*, whereas MCs 6–8, which are more prominent in WT cells, preferentially expressed genes related to differentiation and development processes, such as *Emp1*, *Tgm3*, and *Adap1* (Figure 4D). Accordingly, while we did not note any general effect of *Meteor* KO on the levels of classic pluripotency markers such as *Oct4*, *Sox2*, and *Nanog* in bulk RNA-seq, we did observe upregulation of genes normally associated with the pluripotent state and downregulation of genes that are normally associated with more differentiated states (Figure S4F).

The total number of cells occupying the more differentiated subset of the *Meteor* pKO population (MCs 2–4; Figure S4B) did not significantly change. However, similarly to the shift within the pluripotency-related population, there was a shift within these MCs, with *Meteor* pKO cells occupying MC 4 rather than MCs 2–3, which were populated predominantly by WT cells (Figures 4C, S4B, and S4E). The expression of *Eomes* itself was highest in MC 2 (Figures 4B and S4B), which is associated with high expression of genes involved in mesoderm specification such as *T*, *Mesp1*, *Mixl1*, and *Gsc* (Figure 4E). The reduction of cells occupying MC 2 was thus the likely cause for both the reduction of total *Eomes* levels seen in the bulk RNA-seq (Figure 1C) as well as the reduced capacity of serum-grown mESCs to differentiate into cardiac mesoderm genes previously noted.[20,33] The fact that *Meteor* KO caused a decrease in cells from MCs in which *Meteor* itself was not expressed at significant levels (Figures 4B, 4C, S4B, and S4E) suggests that either *Meteor* RNA is dispensable for the establishment of the cellular states represented by these MCs—making the DNA element the functional feature of *Meteor* in this system—or, alternatively, that cells cycle back and forth between the different states, with *Meteor* repression in the pluripotency-related states preventing their entering the state represented by MCs 2 and 3, possibly mediated by epigenetic changes that we observed in the *Meteor* locus (Figures 2A and 2B) (see discussion).

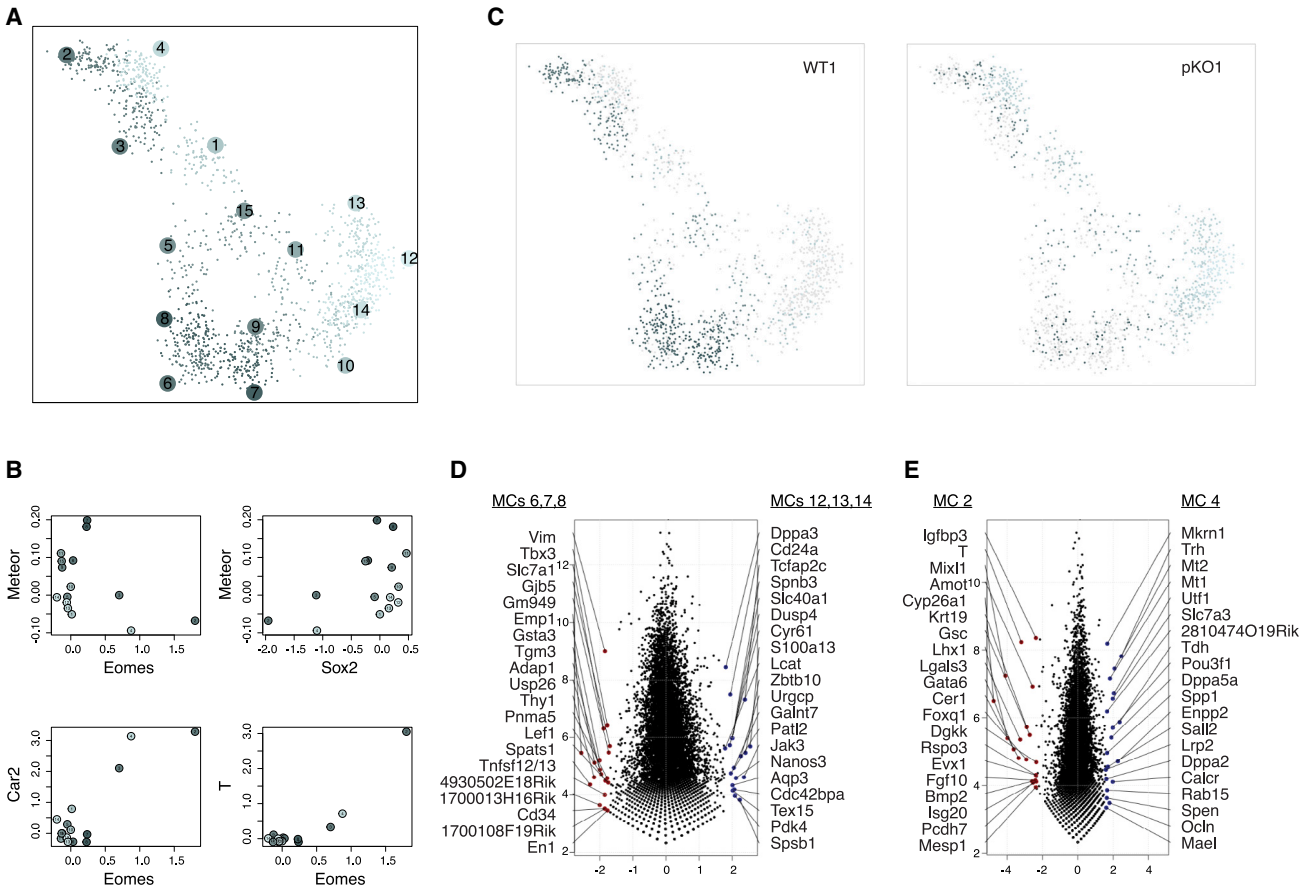

Figure 4. Distinct subpopulations of mESCs in *Meteor* WT and KO mESCs

(A) 2D projection of the MetaCell[60] adjacency graph. Cells are shown as small dots, whose location indicates similarity to the adjacent cells and metacells (MCs). Color was assigned to each MC according to the ratio of WT and pKO cells that comprise it, with darker shades representing MCs comprised mostly of WT cells and lighter shades representing MCs comprised mostly of pKO cells.

(B) Correlation between the log of the fold enrichment values (expression enrichment over the median MC) for the indicated gene pairs, separated by MCs.

(C) Same as (A), separately for WT1 and pKO1 cells.

(D) Scatterplot comparing gene expression between the indicated groups of MCs. Highlighted are the 20 most differentially expressed genes in each group.

(E) Same as (D), for MCs 2 and 4.

See also Figure S4.

A distinct functional feature in *Meteor* represses *Eomes* in NPCs

As opposed to MC 2, MC 4, which was substantially more populated in the *Meteor* KO population compared with WT cells, did not express predominantly mesoderm-related genes but was rather defined by an enrichment of genes associated with neurogenesis such as *Pou3f1*, *Sall2*, *Trh*, and *Rab15* (Figure 4E). It was previously suggested that the reduced mesodermal differentiation capacity of *Meteor* KO cells drives them toward the neuronal lineage.[20] We therefore examined whether *Meteor* repression had an effect on the ability of mESCs to differentiate into neurons. In contrast to the EB differentiation system, where *Meteor* was rapidly reduced to undetectable levels (Figure S3A), *Meteor* continued to be expressed throughout neuronal differentiation (using a two-step differentiation protocol described by Ying et al.[64]), albeit with reduced expression levels, an expression pattern that correlated with *Eomes* expression in this system (Figures 5A and 5B). The chromatin organization of the locus also changed throughout the differentiation system, with *Meteor-Eomes* contacts remaining stable in neural progenitor cells (NPCs) but decreasing at day 8 of neuronal differentiation (Figure 5A). Active regions within the locus also shifted throughout the differentiation system, with the *Golga4* promoter—which is found in significant spatial proximity to *Eomes* in neurons (Figure 5A)—being the most active region in NPCs, as indicated by H3K27ac ChIP-seq we performed in these cells (Figure 5C). This draws a correlation between *Eomes* expression and spatial proximity to the *Meteor* locus throughout neuronal differentiation and suggests that distinct *cis* elements regulate *Eomes* expression in this system, with the *Meteor* lncRNA or its underlying enhancer possibly contributing to this regulation.

Accordingly, we tested the ability of *Meteor* KO mESCs to undergo neuronal differentiation. Both *Meteor* pKO and pInv mESCs were able to differentiate to neurons, as seen by their

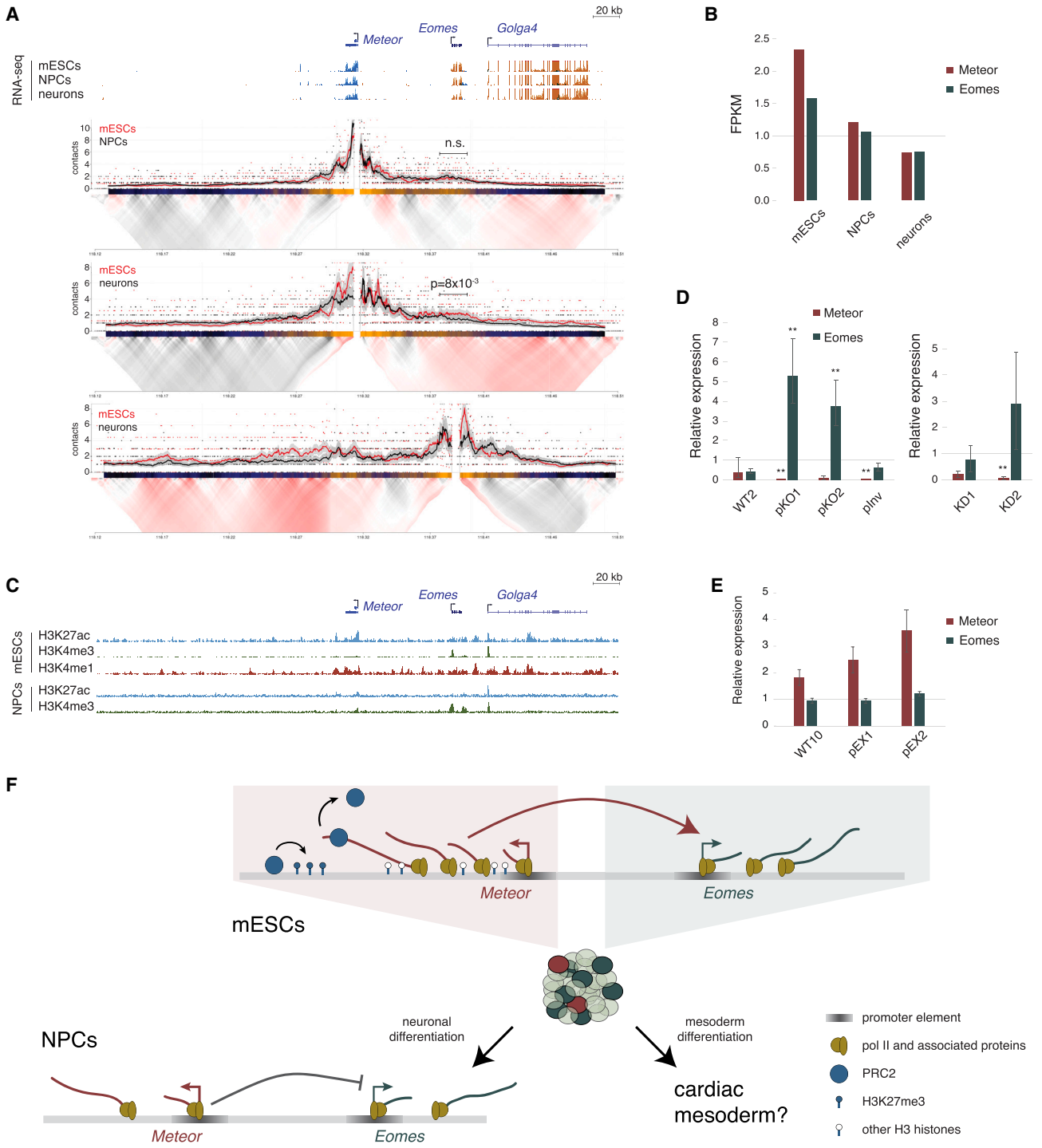

Figure 5. A distinct functional feature of the *Meteor* locus represses *Eomes* throughout neuronal differentiation

(A) (Top) Genome browser image of the region surrounding the *Meteor* locus. Shown are representative transcript models, and RNA-seq tracks taken from Hezroni et al.[65] where orange denotes transcription on the plus strand and blue denotes transcription on the minus strand. All tracks are normalized to the same scale. (Bottom) 4C analysis in the indicated cells using the *Meteor* or *Eomes* promoters as viewpoints. Domainograms showing mean contact per fragment end for a series of window sizes are placed below smoothed trend lines and raw counts of the contact profiles.

(B) RSEM quantifications of *Meteor* and *Eomes* expression levels in the indicated cell types; RNA-seq data are the same as shown in (A).

(C) ENCODE ChIP-seq tracks in mESCs (top), and H3K27ac ChIP-seq and H3K4me3 Cut&Run tracks in NPCs (bottom). Genomic coordinates are aligned to (A).

(legend continued on next page)

ability to form Nestin-expressing NPCs and Tuj1-expressing neurons (Figures S5A and S5B). Surprisingly, however, when *Meteor* pKO cells were differentiated to NPCs, a strong upregulation of *Eomes* expression was noted (Figure 5D). Many genes associated with *Eomes* were also upregulated in the *Meteor* KO NPCs, including genes related to differentiation (such as *Nodal*, *Fgf4*, *Fgf8*, and *FoxA2*). The only GO term category significantly associated with *Eomes* upregulation in these cells was neuronal differentiation, in accordance with the known roles of EOMES in the regulation of neuronal development and differentiation.[21]

Eomes was upregulated in NPCs only when the *Meteor* promoter was deleted, but not inverted (Figure 5D). This is in contrast to the reduced level of *Eomes* seen in mESCs with an inverted *Meteor* promoter (Figure 1C), suggesting that a distinct functional feature mediates *Meteor* activity in mESCs as compared with NPCs, and also indicating that altered *Eomes* expression in NPCs is not a consequence of the differential *Eomes* expression in mESCs, which was noted in both pKO and pInv cells. Furthermore, *Eomes* levels were not increased when the pEX lines, in which transcription into the *Meteor* gene body was initiated at a constitutive PGK promoter rather than the *Meteor* promoter, were differentiated to NPCs (Figure 5E). A plausible explanation for this observation is competition between the *Eomes* and *Meteor* promoters over the activity of a shared enhancer (see discussion). Consistent with this model, *Meteor* dCas9-KD cells also did not show significant upregulation of *Eomes* upon differentiation to NPCs (Figure 5D), although it is noteworthy that there was some non-significant upregulation of *Eomes* compared with the control in one of the cell lines in which the KD was somewhat more efficient. It thus appears that the DNA element underlying the *Meteor* transcriptional activity is important for proper regulation of *Eomes* levels in NPCs.

DISCUSSION

The low sequence conservation of enhancer-transcribed lncRNAs[8,16,66] suggests that as a group, the RNA products of these genes likely do not play an important role in enhancer activity. Rather, if functional, these loci are proposed to act mostly via their underlying DNA element or by the act of their transcription.[15] Distinguishing between these levels of functionality is notoriously difficult, complicating efforts to reconcile results from different studies on the same gene. Here, we show that the *Meteor* locus encodes for two distinct, cell-type-specific functions, one of which is DNA mediated and the other dependent on the act of transcription through the locus (Figure 5F). In naive mESCs, elongation through the *Meteor* gene body appears to be necessary for maintaining *Eomes* levels, as KO or inversion of the *Meteor* promoter are sufficient to reduce *Eomes* levels by ~50%, whereas dCas9-KD, introduction of Rz or pAS sequences, or promoter replacement—all of which allow some level of transcription through the locus—do not have this effect on *Eomes* levels (Figures 1C–1H). It is noteworthy that the effects of "the act of transcription" may be specific to transcription through a particular region within the lncRNA gene, as has been demonstrated for the *Airn* lncRNA.[67] The effect of Rz-mediated cleavage on the distance and dynamics of transcription after the Rz sequence has been encountered is not yet clear and might depend on local sequence attributes that dictate folding dynamics. Similarly, the transcription machinery has been suggested to continue transcribing for a few kilobases after encountering a pAS.[68] Thus, the lack of a significant effect on *Eomes* levels caused by insertion of a pAS or Rz sequence into the first intron or second exon of *Meteor*, respectively (Figures 1A, 1D, and 1F) does not necessarily indicate that transcription through the remainder of the locus is dispensable for full functionality, nor does it contradict the phenotype observed upon insertion of a pAS further downstream of the *Meteor* TSS.[20]

The reduced *Eomes* expression in *Meteor* pKO lines is accompanied by H3K27me3 accumulation around the broad enhancer region within the *Meteor* locus (Figures 2B and S2E). Combined with the association of *Meteor* lncRNA with PRC2 (Figures 2C and S2F), this suggests that as *Meteor* is being transcribed its association with PRC2 evicts the latter from the DNA and prevents H3K27me3 deposition, in accordance with previous findings that the binding of PRC2 to DNA and RNA is mutually exclusive.[47–50] Importantly, functionality of the act of transcription may also include the nascent RNA produced in the process—for example, by recruiting or evicting proteins such as PRC2 from the chromatin, as has been proposed[69]—with the lingering RNA present at the end of the transcriptional process being dispensable for the activity. It is not yet clear in what way the increased H3K27me3 accumulation around the *Meteor* enhancer is translated into reduced *Eomes* expression and whether this involves PRC2's role in mediating spatial chromatin organization in mESCs,[44–46] as might be suggested by the reduced contacts between the *Eomes* and *Meteor* regions in *Meteor* KO cells (Figures 2A and S2B). Regardless of the exact mechanism, however, the association of PRC2 with *Meteor* does not necessarily imply a sequence-specific function of *Meteor*, as the selectivity and specificity of PRC2's interaction with RNA is unclear.[70–74]

Intriguingly, inhibition of *Meteor* transcription elongation in mESCs causes reduction in *Eomes* levels despite the two transcripts being expressed in largely distinct cells within the mESC population (Figures 4B, S4B, and S4C), suggesting that

(D) DESeq2 quantifications of *Meteor* and *Eomes* in NPCs derived from the indicated cell lines. Amounts normalized to WT1/Ctrl. Bars represent standard errors; n = 3. $^{**}p_{adj} < 0.005$.

(E) qRT-PCR quantifications of *Meteor* and *Eomes* in NPCs derived from the indicated cell lines. Levels were normalized to WT9 and *Ppib* for internal control. Bars represent standard errors; n = 3.

(F) Model of *Meteor* function. In mESCs, the *Meteor* locus activates *Eomes* expression. Perturbing elongation through the locus is associated with increased H3K27me3 deposition and decreased *Eomes* expression, likely through decreasing the *Eomes*-expressing mESC subpopulation. As a function of the growth conditions of the cells, this might result in reduced efficiency of cardiac mesoderm formation. Following neuronal differentiation, the *Meteor* locus now represses *Eomes* levels, with the DNA element or transcription initiation serving as the functional feature.

See also Figure S5.

Meteor transcription indirectly regulates *Eomes* by affecting the state at which the cells are found. This model can also explain the apparently different effects of *Meteor* inhibition on the ability of mESCs to differentiate to beating EBs, which was unaffected in our hands when growing mESCs in 2i but severely affected in *Meteor*-null cells grown in serum.[20,33] This indicates that *Meteor* repression affects the differentiation potential of the population when grown under specific conditions rather than the hindered differentiation ability being a direct consequence of reduced *Eomes* levels. This altered differentiation potential can be linked to the altered epigenetic landscape in *Meteor* pKO and pInv cells (Figures 2A and 2B), which could itself prevent mESCs from entering or remaining in a cellular state that requires *Eomes* expression, affecting the overall level of *Eomes* expression detected in bulk RNA-seq. This exemplifies how transcription of lncRNA loci could participate in priming differentiation or developmental processes during which they are no longer required to be expressed. Interestingly, an additional pluripotency-associated lncRNA, *Platr4*, was recently shown to act in *trans* to promote mesoderm differentiation *in vitro* and *in vivo* while itself being rapidly downregulated during differentiation, suggesting that such priming activities by lncRNAs might be common in early development.[75]

In contrast to the situation in mESCs, during neuronal differentiation the *Meteor* locus acts to repress, rather than enhance, *Eomes* expression (Figures 5D and 5F). Also contrary to its function in mESCs, the functional feature of *Meteor* in this system appears to be the DNA element—specifically, the short region that encompasses the TSS and first exon of the lncRNA—rather than elongation through the *Meteor* enhancer, as no changes in *Eomes* expression in NPCs are noted when the *Meteor* promoter is inverted (Figure 5D). The mechanism through which *Meteor* represses *Eomes* in this system is not yet clear, although considering the dependency of the phenotype on the DNA rather the RNA element and the lack of effect when the promoter sequence is severely disrupted by insertion of an alternative promoter and a hygromycin gene (Figure 5E), a particularly appealing possibility is competition between the *Eomes* and *Meteor* loci over binding to enhancers, as has been shown for other lncRNA loci.[76] A possible candidate for the limiting enhancer is the region downstream of *Eomes* with which the *Eomes* locus is associated following neuronal differentiation (Figure 5A). Regardless of the mechanism, the consequence of the heightened *Eomes* expression in *Meteor*-null NPCs, and specifically whether it affects the efficiency of neuronal differentiation, remains to be seen. Alternatively, as *Eomes* is expressed only at specific times and compartments within the developing brain,[21] increased *Eomes* expression in NPCs could affect the composition of the neuronal types acquired throughout the differentiation process, implicating the *Meteor* enhancer in fine-tuning neuronal differentiation.

The study of *Meteor* illustrates the importance of careful selection of perturbation techniques for the study of lncRNA loci, as both the suggested function and functional feature of the locus appear to depend on the employed perturbation method. Taken together, the emerging picture is that *Meteor* controls *Eomes* levels through distinct, cell-type-specific functional features, but not through its RNA product. While our findings do not exclude the possibility that the *Meteor* locus has additional functions in other systems or through additional functional features, as has been suggested,[33] we could not detect any substantial *Meteor* expression in systems other than mESCs, testes, and throughout neuronal differentiation (Figures S3A, 5A, and 5B; https://bis.zju.edu.cn/MCA/search3.html), which makes an RNA-dependent *Meteor* function in other cell types unlikely. The lack of an RNA-based function is also consistent with our inability to identify sequence-similar homologs of the *Meteor* lncRNA outside of rodents. The human lncRNA *LINC01980* is transcribed from a syntenic region and has a similar expression pattern,[20] but when its sequence is projected to the mouse genome through a whole-genome alignment it does not overlap with the *Meteor* locus.

The intricate, cell-type-specific regulation of *Eomes* through distinct features of the *Meteor* locus serves as an illustration of how complex regulation of master regulator TFs can be fine-tuned through the use of lncRNA transcriptional units. This can be achieved through combinatorial activity of multiple lncRNA units, as has been described for the regulatory network of the *Hand2* TF[17,77] or, as described here, through distinct functions mediated by the same locus in different cellular contexts. It is expected that in-depth study of additional lncRNA loci, using multiple perturbations in various biological systems, will uncover additional loci with complex phenotypical output and unveil other mechanisms through which lncRNA loci contribute to regulation of gene expression.

LIMITATIONS OF THE STUDY

In contrast to several previous studies of *Meteor* lncRNA, we show here that *Meteor*-null mESCs can efficiently differentiate to cardiac mesoderm. To ascertain whether different initial growth conditions of the mESCs, and not clonal selection, indeed explain these variations, further experiments would be needed, including differentiation of our KO cells after growing them in serum-based media. Furthermore, we currently compare the effects of *Meteor* depletion on early mesoderm differentiation and on NPCs, which comprise a more differentiated state along the ectoderm lineage. In the future, it would be interesting to look at earlier stages of ectoderm differentiation, potentially with single-cell resolution, so as to directly compare the results with findings relating to mesoderm differentiation and to ascertain whether the changes in the *Eomes*-expressing subpopulation of the mESCs have an effect on differentiation to additional germ layers.

Furthermore, additional cellular models can help validate and identify other functional features of the *Meteor* locus. Specifically, replacing the *Meteor* promoter with a different, sequence-diverged yet transcriptionally active promoter might help validate our findings regarding the DNA element being the functional feature of *Meteor* in NPCs. Nonetheless, as clean separation of the effects of a DNA from any transcriptional activity is challenging, and as another promoter might contain some sequence elements in common with the *Meteor* promoter, a library of mutated *Meteor* promoter sequences would enable zeroing in on the exact sequence elements that confer the promoter activity. Lastly, this study focused on the roles of different

functional features within the *Meteor* locus *in vitro*; further studies are needed to delineate their contribution to early embryonic development *in vivo*.

STAR★METHODS

Detailed methods are provided in the online version of this paper and include the following:

- KEY RESOURCES TABLE
- RESOURCE AVAILABILITY
  - Lead contact
  - Materials availability
  - Data and code availability
- EXPERIMENTAL MODEL AND STUDY PARTICIPANT DETAILS
- METHOD DETAILS
  - Generation of promoter KO (pKO) and inversion (pInv) cell lines
  - Generation of polyA insertion (pAS) cell lines
  - Generation of PGK promoter exchange (pEX) cell lines
  - Generation of dCas9-KD cell lines
  - EB differentiation
  - Neuronal differentiation
  - RNA sequencing
  - Chromatin immunoprecipitation (ChIP)
  - Cut&Run
  - Targeted chromosome conformation capture (4C)
- QUANTIFICATION AND STATISTICAL ANALYSIS
  - Statistical analyses
  - Cut&Run data analysis

SUPPLEMENTAL INFORMATION

Supplemental information can be found online at https://doi.org/10.1016/j.celrep.2023.112569.

ACKNOWLEDGMENTS

We thank the Weizmann Institute Stem Cells facility for assistance with generating the *Meteor* pEX and pAS cell lines. We thank Yonatan Stelzer and Phillip Grote for helpful discussions and members of the Ulitsky lab for helpful discussions and comments on the manuscript. We thank Amos Tanay and members of the Tanay lab for discussions on 4C and on analysis of scRNA-seq and Eyal David for discussions on analysis of 3′ RNA-seq. We thank Jacob Hanna, Nofar Mor, and members of the Hanna lab, as well as Yossi Buganim and Mufeed Abdeen, for discussions on mESC growth conditions. We thank Liat Fellus Alyagor and Dana Hirsch for their help with single-molecule fluorescence *in situ* hybridization experiments. This study was supported by grants to I.U. from the European Research Council Consolidator grant program (lncIMPACT project) and from the Helen and Martin Kimmel Institute for Stem Cell Research. Z.M. is the incumbent of the anonymous Europe Endowment for Research Fellow Chair in artificial intelligence, and R.B.-T.P. is the incumbent of the Arlyn Imberman Research Fellow Chair.

AUTHOR CONTRIBUTIONS

N.G. and I.U. conceived the study. N.G. and R.B.-T.P. carried out experiments. N.G. analyzed all high-throughput data. Z.M. assisted with generating scRNA-seq libraries. A.T. and M.B. generated the *Meteor* fKO and Rz-KD model. N.G. and I.U. wrote the manuscript with input from the other authors.

DECLARATION OF INTERESTS

I.U. is a member of the *Cell Reports* advisory board.

Received: November 10, 2020
Revised: March 7, 2023
Accepted: May 12, 2023
Published: May 31, 2023

REFERENCES

1. Guttman, M., Amit, I., Garber, M., French, C., Lin, M.F., Feldser, D., Huarte, M., Zuk, O., Carey, B.W., Cassady, J.P., et al. (2009). Chromatin signature reveals over a thousand highly conserved large non-coding RNAs in mammals. Nature *458*, 223–227.
2. Mercer, T.R., Gerhardt, D.J., Dinger, M.E., Crawford, J., Trapnell, C., Jeddeloh, J.A., Mattick, J.S., and Rinn, J.L. (2011). Targeted RNA sequencing reveals the deep complexity of the human transcriptome. Nat. Biotechnol. *30*, 99–104.
3. Carninci, P., Kasukawa, T., Katayama, S., Gough, J., Frith, M.C., Maeda, N., Oyama, R., Ravasi, T., Lenhard, B., Wells, C., et al. (2005). The transcriptional landscape of the mammalian genome. Science *309*, 1559–1563.
4. Sherstyuk, V.V., Medvedev, S.P., and Zakian, S.M. (2018). Noncoding RNAs in the regulation of pluripotency and reprogramming. Stem Cell Rev. Rep. *14*, 58–70.
5. Guttman, M., Donaghey, J., Carey, B.W., Garber, M., Grenier, J.K., Munson, G., Young, G., Lucas, A.B., Ach, R., Bruhn, L., et al. (2011). lincRNAs act in the circuitry controlling pluripotency and differentiation. Nature *477*, 295–300.
6. Vučićević, D., Corradin, O., Ntini, E., Scacheri, P.C., and Ørom, U.A. (2015). Long ncRNA expression associates with tissue-specific enhancers. Cell Cycle *14*, 253–260.
7. De Santa, F., Barozzi, I., Mietton, F., Ghisletti, S., Polletti, S., Tusi, B.K., Muller, H., Ragoussis, J., Wei, C.-L., and Natoli, G. (2010). A large fraction of extragenic RNA pol II transcription sites overlap enhancers. PLoS Biol. *8*, e1000384.
8. Marques, A.C., Hughes, J., Graham, B., Kowalczyk, M.S., Higgs, D.R., and Ponting, C.P. (2013). Chromatin signatures at transcriptional start sites separate two equally populated yet distinct classes of intergenic long noncoding RNAs. Genome Biol. *14*, R131.
9. Xiang, J.-F., Yin, Q.-F., Chen, T., Zhang, Y., Zhang, X.-O., Wu, Z., Zhang, S., Wang, H.-B., Ge, J., Lu, X., et al. (2014). Human colorectal cancer-specific CCAT1-L lncRNA regulates long-range chromatin interactions at the MYC locus. Cell Res. *24*, 513–531.
10. Lai, F., Orom, U.A., Cesaroni, M., Beringer, M., Taatjes, D.J., Blobel, G.A., and Shiekhattar, R. (2013). Activating RNAs associate with Mediator to enhance chromatin architecture and transcription. Nature *494*, 497–501.
11. Fanucchi, S., Fok, E.T., Dalla, E., Shibayama, Y., Börner, K., Chang, E.Y., Stoychev, S., Imakaev, M., Grimm, D., Wang, K.C., et al. (2019). Immune genes are primed for robust transcription by proximal long noncoding RNAs located in nuclear compartments. Nat. Genet. *51*, 138–150.
12. Isoda, T., Moore, A.J., He, Z., Chandra, V., Aida, M., Denholtz, M., Piet van Hamburg, J., Fisch, K.M., Chang, A.N., Fahl, S.P., et al. (2017). Non-coding transcription instructs chromatin folding and compartmentalization to dictate enhancer-promoter communication and T cell fate. Cell *171*, 103–119.e18.
13. Gil, N., and Ulitsky, I. (2018). Production of spliced long noncoding RNAs specifies regions with increased enhancer activity. Cell Syst. *7*, 537–547.e3.
14. Engreitz, J.M., Haines, J.E., Perez, E.M., Munson, G., Chen, J., Kane, M., McDonel, P.E., Guttman, M., and Lander, E.S. (2016). Local regulation of gene expression by lncRNA promoters, transcription and splicing. Nature *539*, 452–455.

15. Gil, N., and Ulitsky, I. (2020). Regulation of gene expression by cis-acting long non-coding RNAs. Nat. Rev. Genet. *21*, 102–117.

16. Ulitsky, I. (2016). Evolution to the rescue: using comparative genomics to understand long non-coding RNAs. Nat. Rev. Genet. *17*, 601–614.

17. Anderson, K.M., Anderson, D.M., McAnally, J.R., Shelton, J.M., Bassel-Duby, R., and Olson, E.N. (2016). Transcription of the non-coding RNA upperhand controls Hand2 expression and heart development. Nature *539*, 433–436.

18. Han, X., Zhang, J., Liu, Y., Fan, X., Ai, S., Luo, Y., Li, X., Jin, H., Luo, S., Zheng, H., et al. (2019). The lncRNA Hand2os1/Uph locus orchestrates heart development through regulation of precise expression of Hand2. Development *146*, dev176198. https://doi.org/10.1242/dev.176198.

19. Bergmann, J.H., Li, J., Eckersley-Maslin, M.A., Rigo, F., Freier, S.M., and Spector, D.L. (2015). Regulation of the ESC transcriptome by nuclear long noncoding RNAs. Genome Res. *25*, 1336–1346.

20. Alexanian, M., Maric, D., Jenkinson, S.P., Mina, M., Friedman, C.E., Ting, C.-C., Micheletti, R., Plaisance, I., Nemir, M., Maison, D., et al. (2017). A transcribed enhancer dictates mesendoderm specification in pluripotency. Nat. Commun. *8*, 1806.

21. Mihalas, A.B., and Hevner, R.F. (2017). Control of neuronal development by T-box genes in the brain. Curr. Top. Dev. Biol. *122*, 279–312.

22. Probst, S., and Arnold, S.J. (2017). Eomesodermin-at dawn of cell fate decisions during early embryogenesis. Curr. Top. Dev. Biol. *122*, 93–115.

23. Kidder, B.L., and Palmer, S. (2010). Examination of transcriptional networks reveals an important role for TCFAP2C, SMARCA4, and EOMES in trophoblast stem cell maintenance. Genome Res. *20*, 458–472.

24. Russ, A.P., Wattler, S., Colledge, W.H., Aparicio, S.A., Carlton, M.B., Pearce, J.J., Barton, S.C., Surani, M.A., Ryan, K., Nehls, M.C., et al. (2000). Eomesodermin is required for mouse trophoblast development and mesoderm formation. Nature *404*, 95–99.

25. Strumpf, D., Mao, C.-A., Yamanaka, Y., Ralston, A., Chawengsaksophak, K., Beck, F., and Rossant, J. (2005). Cdx2 is required for correct cell fate specification and differentiation of trophectoderm in the mouse blastocyst. Development *132*, 2093–2102.

26. Ciruna, B.G., and Rossant, J. (1999). Expression of the T-box gene Eomesodermin during early mouse development. Mech. Dev. *81*, 199–203.

27. Hancock, S.N., Agulnik, S.I., Silver, L.M., and Papaioannou, V.E. (1999). Mapping and expression analysis of the mouse ortholog of Xenopus Eomesodermin. Mech. Dev. *81*, 205–208.

28. Lv, X., Ren, S.-Q., Zhang, X.-J., Shen, Z., Ghosh, T., Xianyu, A., Gao, P., Li, Z., Lin, S., Yu, Y., et al. (2019). TBR2 coordinates neurogenesis expansion and precise microcircuit organization via Protocadherin 19 in the mammalian cortex. Nat. Commun. *10*, 3946.

29. Gordon, S.M., Chaix, J., Rupp, L.J., Wu, J., Madera, S., Sun, J.C., Lindsten, T., and Reiner, S.L. (2012). The transcription factors T-bet and Eomes control key checkpoints of natural killer cell maturation. Immunity *36*, 55–67.

30. Pearce, E.L., Mullen, A.C., Martins, G.A., Krawczyk, C.M., Hutchins, A.S., Zediak, V.P., Banica, M., DiCioccio, C.B., Gross, D.A., Mao, C.-A., et al. (2003). Control of effector CD8+ T cell function by the transcription factor Eomesodermin. Science *302*, 1041–1043.

31. Zhu, Y., Ju, S., Chen, E., Dai, S., Li, C., Morel, P., Liu, L., Zhang, X., and Lu, B. (2010). T-bet and eomesodermin are required for T cell-mediated antitumor immune responses. J. Immunol. *185*, 3174–3183.

32. Simon, C.S., Downes, D.J., Gosden, M.E., Telenius, J., Higgs, D.R., Hughes, J.R., Costello, I., Bikoff, E.K., and Robertson, E.J. (2017). Functional characterisation of cis-regulatory elements governing dynamic Eomes expression in the early mouse embryo. Development *144*, 1249–1260.

33. Guo, X., Xu, Y., Wang, Z., Wu, Y., Chen, J., Wang, G., Lu, C., Jia, W., Xi, J., Zhu, S., et al. (2018). A linc1405/eomes complex promotes cardiac mesoderm specification and cardiogenesis. Cell Stem Cell *22*, 893–908.e6.

34. Tuck, A.C., Natarajan, K.N., Rice, G.M., Borawski, J., Mohn, F., Rankova, A., Flemr, M., Wenger, A., Nutiu, R., Teichmann, S., and Bühler, M. (2018). Distinctive features of lincRNA gene expression suggest widespread RNA-independent functions. Life Sci. Alliance *1*, e201800124.

35. Gilbert, L.A., Larson, M.H., Morsut, L., Liu, Z., Brar, G.A., Torres, S.E., Stern-Ginossar, N., Brandman, O., Whitehead, E.H., Doudna, J.A., et al. (2013). CRISPR-mediated modular RNA-guided regulation of transcription in eukaryotes. Cell *154*, 442–451.

36. Guo, G., Pinello, L., Han, X., Lai, S., Shen, L., Lin, T.-W., Zou, K., Yuan, G.-C., and Orkin, S.H. (2016). Serum-based culture conditions provoke gene expression variability in mouse embryonic stem cells as revealed by single-cell analysis. Cell Rep. *14*, 956–965.

37. Marks, H., Kalkan, T., Menafra, R., Denissov, S., Jones, K., Hofemeister, H., Nichols, J., Kranz, A., Stewart, A.F., Smith, A., and Stunnenberg, H.G. (2012). The transcriptional and epigenomic foundations of ground state pluripotency. Cell *149*, 590–604.

38. Joo, J.Y., Choi, H.W., Kim, M.J., Zaehres, H., Tapia, N., Stehling, M., Jung, K.S., Do, J.T., and Schöler, H.R. (2014). Establishment of a primed pluripotent epiblast stem cell in FGF4-based conditions. Sci. Rep. *4*, 7477.

39. Kojima, Y., Kaufman-Francis, K., Studdert, J.B., Steiner, K.A., Power, M.D., Loebel, D.A.F., Jones, V., Hor, A., de Alencastro, G., Logan, G.J., et al. (2014). The transcriptional and functional properties of mouse epiblast stem cells resemble the anterior primitive streak. Cell Stem Cell *14*, 107–120.

40. Castro-Mondragon, J.A., Riudavets-Puig, R., Rauluseviciute, I., Lemma, R.B., Turchi, L., Blanc-Mathieu, R., Lucas, J., Boddie, P., Khan, A., Manosalva Pérez, N., et al. (2022). Jaspar 2022: the 9th release of the open-access database of transcription factor binding profiles. Nucleic Acids Res. *50*, D165–D173.

41. Bailey, T.L., Boden, M., Buske, F.A., Frith, M., Grant, C.E., Clementi, L., Ren, J., Li, W.W., and Noble, W.S. (2009). Meme suite: tools for motif discovery and searching. Nucleic Acids Res. *37*, W202–W208.

42. Schwartzman, O., Mukamel, Z., Oded-Elkayam, N., Olivares-Chauvet, P., Lubling, Y., Landan, G., Izraeli, S., and Tanay, A. (2016). UMI-4C for quantitative and targeted chromosomal contact profiling. Nat. Methods *13*, 685–691.

43. Zhao, J., Ohsumi, T.K., Kung, J.T., Ogawa, Y., Grau, D.J., Sarma, K., Song, J.J., Kingston, R.E., Borowsky, M., and Lee, J.T. (2010). Genome--wide identification of polycomb-associated RNAs by RIP-seq. Mol. Cell *40*, 939–953.

44. Cruz-Molina, S., Respuela, P., Tebartz, C., Kolovos, P., Nikolic, M., Fueyo, R., van Ijcken, W.F.J., Grosveld, F., Frommolt, P., Bazzi, H., and Rada-Iglesias, A. (2017). PRC2 facilitates the regulatory topology required for poised enhancer function during pluripotent stem cell differentiation. Cell Stem Cell *20*, 689–705.e9.

45. Denholtz, M., Bonora, G., Chronis, C., Splinter, E., de Laat, W., Ernst, J., Pellegrini, M., and Plath, K. (2013). Long-range chromatin contacts in embryonic stem cells reveal a role for pluripotency factors and polycomb proteins in genome organization. Cell Stem Cell *13*, 602–616.

46. Ngan, C.Y., Wong, C.H., Tjong, H., Wang, W., Goldfeder, R.L., Choi, C., He, H., Gong, L., Lin, J., Urban, B., et al. (2020). Chromatin interaction analyses elucidate the roles of PRC2-bound silencers in mouse development. Nat. Genet. *52*, 264–272.

47. Beltran, M., Tavares, M., Justin, N., Khandelwal, G., Ambrose, J., Foster, B.M., Worlock, K.B., Tvardovskiy, A., Kunzelmann, S., Herrero, J., et al. (2019). G-tract RNA removes Polycomb repressive complex 2 from genes. Nat. Struct. Mol. Biol. *26*, 899–909.

48. Beltran, M., Yates, C.M., Skalska, L., Dawson, M., Reis, F.P., Viiri, K., Fisher, C.L., Sibley, C.R., Foster, B.M., Bartke, T., et al. (2016). The interaction of PRC2 with RNA or chromatin is mutually antagonistic. Genome Res. *26*, 896–907.

49. Hosogane, M., Funayama, R., Shirota, M., and Nakayama, K. (2016). Lack of transcription triggers H3K27me3 accumulation in the gene body. Cell Rep. *16*, 696–706.

50. Kaneko, S., Son, J., Bonasio, R., Shen, S.S., and Reinberg, D. (2014). Nascent RNA interaction keeps PRC2 activity poised and in check. Genes Dev. *28*, 1983–1988.

51. Garland, W., Comet, I., Wu, M., Radzisheuskaya, A., Rib, L., Vitting-Seerup, K., Lloret-Llinares, M., Sandelin, A., Helin, K., and Jensen, T.H. (2019). A functional link between nuclear RNA decay and transcriptional control mediated by the polycomb repressive complex 2. Cell Rep. *29*, 1800–1811.e6.

52. Maltsev, V.A., Wobus, A.M., Rohwedel, J., Bader, M., and Hescheler, J. (1994). Cardiomyocytes differentiated in vitro from embryonic stem cells developmentally express cardiac-specific genes and ionic currents. Circ. Res. *75*, 233–244.

53. Guan, K., Rohwedel, J., and Wobus, A.M. (1999). Embryonic stem cell differentiation models: cardiogenesis, myogenesis, neurogenesis, epithelial and vascular smooth muscle cell differentiation in vitro. Cytotechnology *30*, 211–226.

54. He, Z., Li, J.-J., Zhen, C.-H., Feng, L.-Y., and Ding, X.-Y. (2006). Effect of leukemia inhibitory factor on embryonic stem cell differentiation: implications for supporting neuronal differentiation. Acta Pharmacol. Sin. *27*, 80–90.

55. Gajović, S., St-Onge, L., Yokota, Y., and Gruss, P. (1997). Retinoic acid mediates Pax6 expression during in vitro differentiation of embryonic stem cells. Differentiation. *62*, 187–192.

56. Gaztelumendi, N., and Nogués, C. (2014). Chromosome instability in mouse embryonic stem cells. Sci. Rep. *4*, 5324.

57. Keller, A., and Spits, C. (2021). The impact of acquired genetic abnormalities on the clinical translation of human pluripotent stem cells. Cells *10*. https://doi.org/10.3390/cells10113246.

58. Hayashi, K., de Sousa Lopes, S.M.C., Tang, F., Lao, K., and Surani, M.A. (2008). Dynamic equilibrium and heterogeneity of mouse pluripotent stem cells with distinct functional and epigenetic states. Cell Stem Cell *3*, 391–401.

59. Choi, J., Huebner, A.J., Clement, K., Walsh, R.M., Savol, A., Lin, K., Gu, H., Di Stefano, B., Brumbaugh, J., Kim, S.-Y., et al. (2017). Prolonged Mek1/2 suppression impairs the developmental potential of embryonic stem cells. Nature *548*, 219–223.

60. Baran, Y., Bercovich, A., Sebe-Pedros, A., Lubling, Y., Giladi, A., Chomsky, E., Meir, Z., Hoichman, M., Lifshitz, A., and Tanay, A. (2019). MetaCell: analysis of single-cell RNA-seq data using K-nn graph partitions. Genome Biol. *20*, 206.

61. Perea-Gomez, A., Lawson, K.A., Rhinn, M., Zakin, L., Brûlet, P., Mazan, S., and Ang, S.L. (2001). Otx2 is required for visceral endoderm movement and for the restriction of posterior signals in the epiblast of the mouse embryo. Development *128*, 753–765.

62. Perea-Gómez, A., Shawlot, W., Sasaki, H., Behringer, R.R., and Ang, S. (1999). HNF3beta and Lim1 interact in the visceral endoderm to regulate primitive streak formation and anterior-posterior polarity in the mouse embryo. Development *126*, 4499–4511.

63. Rivera-Pérez, J.A., and Magnuson, T. (2005). Primitive streak formation in mice is preceded by localized activation of Brachyury and Wnt3. Dev. Biol. *288*, 363–371.

64. Ying, Q.-L., Stavridis, M., Griffiths, D., Li, M., and Smith, A. (2003). Conversion of embryonic stem cells into neuroectodermal precursors in adherent monoculture. Nat. Biotechnol. *21*, 183–186.

65. Hezroni, H., Ben-Tov Perry, R., Gil, N., Degani, N., and Ulitsky, I. (2020). Regulation of neuronal commitment in mouse embryonic stem cells by the Reno1/Bahcc1 locus. EMBO Rep. *21*, e51264.

66. Hezroni, H., Koppstein, D., Schwartz, M.G., Avrutin, A., Bartel, D.P., and Ulitsky, I. (2015). Principles of long noncoding RNA evolution derived from direct comparison of transcriptomes in 17 species. Cell Rep. *11*, 1110–1122.

67. Latos, P.A., Pauler, F.M., Koerner, M.V., Şenergin, H.B., Hudson, Q.J., Stocsits, R.R., Allhoff, W., Stricker, S.H., Klement, R.M., Warczok, K.E., et al. (2012). Airn transcriptional overlap, but not its lncRNA products, induces imprinted Igf2r silencing. Science *338*, 1469–1472.

68. Nojima, T., Gomes, T., Grosso, A.R.F., Kimura, H., Dye, M.J., Dhir, S., Carmo-Fonseca, M., and Proudfoot, N.J. (2015). Mammalian NET-seq reveals genome-wide nascent transcription coupled to RNA processing. Cell *161*, 526–540.

69. Long, Y., Hwang, T., Gooding, A.R., Goodrich, K.J., Rinn, J.L., and Cech, T.R. (2020). RNA is essential for PRC2 chromatin occupancy and function in human pluripotent stem cells. Nat. Genet. *52*, 931–938.

70. Cifuentes-Rojas, C., Hernandez, A.J., Sarma, K., and Lee, J.T. (2014). Regulatory interactions between RNA and polycomb repressive complex 2. Mol. Cell *55*, 171–185.

71. Colognori, D., Sunwoo, H., Kriz, A.J., Wang, C.-Y., and Lee, J.T. (2019). Xist deletional analysis reveals an interdependency between xist RNA and polycomb complexes for spreading along the inactive X. Mol. Cell *74*, 101–117.e10.

72. Davidovich, C., Zheng, L., Goodrich, K.J., and Cech, T.R. (2013). Promiscuous RNA binding by Polycomb repressive complex 2. Nat. Struct. Mol. Biol. *20*, 1250–1257.

73. Wang, X., Goodrich, K.J., Gooding, A.R., Naeem, H., Archer, S., Paucek, R.D., Youmans, D.T., Cech, T.R., and Davidovich, C. (2017). Targeting of polycomb repressive complex 2 to RNA by short repeats of consecutive guanines. Mol. Cell *65*, 1056–1067.e5.

74. Mattick, J.S., Amaral, P.P., Carninci, P., Carpenter, S., Chang, H.Y., Chen, L.-L., Chen, R., Dean, C., Dinger, M.E., Fitzgerald, K.A., et al. (2023). Long non-coding RNAs: definitions, functions, challenges and recommendations. Nat. Rev. Mol. Cell Biol. https://doi.org/10.1038/s41580-022-00566-8.

75. Hazra, R., Brine, L., Garcia, L., Benz, B., Chirathivat, N., Shen, M.M., Wilkinson, J.E., Lyons, S.K., and Spector, D.L. (2022). Platr4 is an early embryonic lncRNA that exerts its function downstream on cardiogenic mesodermal lineage commitment. Dev. Cell *57*, 2450–2468.e7.

76. Cho, S.W., Xu, J., Sun, R., Mumbach, M.R., Carter, A.C., Chen, Y.G., Yost, K.E., Kim, J., He, J., Nevins, S.A., et al. (2018). Promoter of lncRNA gene PVT1 is a tumor-suppressor DNA boundary element. Cell *173*, 1398–1412.e22.

77. Ritter, N., Ali, T., Kopitchinski, N., Schuster, P., Beisaw, A., Hendrix, D.A., Schulz, M.H., Müller-McNicoll, M., Dimmeler, S., and Grote, P. (2019). The lncRNA locus Handsdown regulates cardiac gene programs and is essential for early mouse development. Dev. Cell *50*, 644–657.e8.

78. Stryjewska, A., Dries, R., Pieters, T., Verstappen, G., Conidi, A., Coddens, K., Francis, A., Umans, L., van IJcken, W.F.J., Berx, G., et al. (2017). Zeb2 regulates cell fate at the exit from epiblast state in mouse embryonic stem cells. Stem. Cells *35*, 611–625.

79. Ding, Q., Regan, S.N., Xia, Y., Oostrom, L.A., Cowan, C.A., and Musunuru, K. (2013). Enhanced efficiency of human pluripotent stem cell genome editing through replacing TALENs with CRISPRs. Cell Stem Cell *12*, 393–394.

80. Koike-Yusa, H., Li, Y., Tan, E.-P., Velasco-Herrera, M.D.C., and Yusa, K. (2014). Genome-wide recessive genetic screening in mammalian cells with a lentiviral CRISPR-guide RNA library. Nat. Biotechnol. *32*, 267–273.

81. Konermann, S., Brigham, M.D., Trevino, A.E., Joung, J., Abudayyeh, O.O., Barcena, C., Hsu, P.D., Habib, N., Gootenberg, J.S., Nishimasu, H., et al. (2015). Genome-scale transcriptional activation by an engineered CRISPR-Cas9 complex. Nature *517*, 583–588.

82. Dobin, A., Davis, C.A., Schlesinger, F., Drenkow, J., Zaleski, C., Jha, S., Batut, P., Chaisson, M., and Gingeras, T.R. (2013). STAR: ultrafast universal RNA-seq aligner. Bioinformatics *29*, 15–21.

83. Li, B., and Dewey, C.N. (2011). RSEM: accurate transcript quantification from RNA-Seq data with or without a reference genome. BMC Bioinf. *12*, 323.

84. Love, M.I., Huber, W., and Anders, S. (2014). Moderated estimation of fold change and dispersion for RNA-seq data with DESeq2. Genome Biol. *15*, 550.

85. Kent, W.J., Zweig, A.S., Barber, G., Hinrichs, A.S., and Karolchik, D. (2010). BigWig and BigBed: enabling browsing of large distributed datasets. Bioinformatics *26*, 2204–2207.

86. Ballarino, M., Cipriano, A., Tita, R., Santini, T., Desideri, F., Morlando, M., Colantoni, A., Carrieri, C., Nicoletti, C., Musarò, A., et al. (2018). Deficiency in the nuclear long noncoding RNA Charme causes myogenic defects and heart remodeling in mice. EMBO J. *37*, e99697. https://doi.org/10.15252/embj.201899697.

87. Yin, Y., Yan, P., Lu, J., Song, G., Zhu, Y., Li, Z., Zhao, Y., Shen, B., Huang, X., Zhu, H., et al. (2015). Opposing roles for the lncRNA Haunt and its genomic locus in regulating HOXA gene activation during embryonic stem cell differentiation. Cell Stem Cell *16*, 504–516.

88. Tiscornia, G., Singer, O., and Verma, I.M. (2006). Production and purification of lentiviral vectors. Nat. Protoc. *1*, 241–245.

89. Ying, Q.-L., and Smith, A.G. (2003). Defined conditions for neural commitment and differentiation. Methods Enzymol. *365*, 327–341.

90. Mittnenzweig, M., Mayshar, Y., Cheng, S., Ben-Yair, R., Hadas, R., Rais, Y., Chomsky, E., Reines, N., Uzonyi, A., Lumerman, L., et al. (2021). A single-embryo, single-cell time-resolved model for mouse gastrulation. Cell *184*, 2825–2842.e22.

91. Jaitin, D.A., Kenigsberg, E., Keren-Shaul, H., Elefant, N., Paul, F., Zaretsky, I., Mildner, A., Cohen, N., Jung, S., Tanay, A., and Amit, I. (2014). Massively parallel single-cell RNA-seq for marker-free decomposition of tissues into cell types. Science *343*, 776–779.

92. Keren-Shaul, H., Kenigsberg, E., Jaitin, D.A., David, E., Paul, F., Tanay, A., and Amit, I. (2019). MARS-seq2.0: an experimental and analytical pipeline for indexed sorting combined with single-cell RNA sequencing. Nat. Protoc. *14*, 1841–1862.

93. Rom, A., Melamed, L., Gil, N., Goldrich, M.J., Kadir, R., Golan, M., Biton, I., Perry, R.B.-T., and Ulitsky, I. (2019). Regulation of CHD2 expression by the Chaserr long noncoding RNA gene is essential for viability. Nat. Commun. *10*, 5092.

94. Blecher-Gonen, R., Barnett-Itzhaki, Z., Jaitin, D., Amann-Zalcenstein, D., Lara-Astiaso, D., and Amit, I. (2013). High-throughput chromatin immunoprecipitation for genome-wide mapping of in vivo protein-DNA interactions and epigenomic states. Nat. Protoc. *8*, 539–554.

95. Meers, M.P., Bryson, T.D., Henikoff, J.G., and Henikoff, S. (2019). Improved CUT&RUN chromatin profiling tools. Elife *8*, e46314. https://doi.org/10.7554/eLife.46314.

96. Janssens, D., and Henikoff, S.: CUT&RUN: Targeted in situ genome-wide profiling with high efficiency for low cell numbers v3 (protocols.io.zcpf2vn). Protocols.io. 10.17504/protocols.io.zcpf2vn.

97. Olivares-Chauvet, P., Mukamel, Z., Lifshitz, A., Schwartzman, O., Elkayam, N.O., Lubling, Y., Deikus, G., Sebra, R.P., and Tanay, A. (2016). Capturing pairwise and multi-way chromosomal conformations using chromosomal walks. Nature *540*, 296–300.

STAR★METHODS

KEY RESOURCES TABLE

REAGENT or RESOURCE	SOURCE	IDENTIFIER
Antibodies		
Rabbit monoclonal anti-H3K27ac (D5E4)	Cell Signaling Technology	Cat#8173; RRID AB_10949503
Rabbit monoclonal anti-CTCF (D31H2)	Cell Signaling Technology	Cat#3418; RRID AB_2086791
Rabbit monoclonal anti-H3K27me3 (C36B11)	Cell Signaling Technology	Cat#9733; RRID AB_2616029
Rabbit monoclonal anti-H3K4me3 (C42D8)	Cell Signaling Technology	Cat#9751; RRID AB_2616028
Critical commercial assays		
SENSE mRNA-Seq Library Prep Kit V2	Lexogen	Cat#001.96
QuantSeq 3′ mRNA-Seq Library Prep Kit FWD	Lexogen	Cat#015.96
Xfect mESC Transfection Reagent	Takara Bio	Cat#631320
Deposited data		
Raw and analyzed RNA-seq data	This study	GEO: GSE223445
Raw and analyzed 3′ RNA-seq data	This study	GEO: GSE223449
Raw and analyzed scRNA-seq data	This study	GEO: GSE223452
Raw and analyzed 4C data	This study	GEO: GSE223451
Raw and analyzed ChIP-seq data	This study	GEO: GSE223447
Raw and analyzed Cut&Run data	This study	GEO: GSE223448
Analyzed data of gene expression levels in different mESC compartments	GEO record GSE99366	GEO: GSE99366
Raw data of control mESCs undergoing neural differentiation	Stryjewska et al.[78]	GEO: GSE75616
Raw data of EZH2 RIP-seq	Zhao et al.[43]	GEO: GSE17064
Raw data of EZH2 and SUZ12 RIP-seq in WT mESCs	Garland et al.[51]	GEO: GSE137491
Experimental models: Cell lines		
M. musculus: WT1: R1 wild type	This study	N/A
M. musculus: WT2: R1, wild type	This study	N/A
M. musculus: WT3: R1, wild type	This study	N/A
M. musculus: pKO1: R1, homozygous KO of *Meteor* promoter	This study	N/A
M. musculus: pKO2: R1, homozygous KO of *Meteor* promoter	This study	N/A
M. musculus: pInv: R1, homozygous inversion of *Meteor* promoter	This study	N/A
M. musculus: WT4: 129-C57Bl/6, wild type	Laboratory of Marc Bühler[34]	N/A
M. musculus: WT5: 129-C57Bl/6, wild type	Laboratory of Marc Bühler[34]	N/A
M. musculus: WT6: 129-C57Bl/6, wild type	Laboratory of Marc Bühler[34]	N/A
M. musculus: fKO1: 129-C57Bl/6, homozygous KO of *Meteor* gene	Laboratory of Marc Bühler[34]	N/A
M. musculus: fKO2: 129-C57Bl/6, homozygous KO of *Meteor* gene	Laboratory of Marc Bühler[34]	N/A
M. musculus: Rz-KD: 129-C57Bl/6, homozygous insertion of a Rz sequence into *Meteor*	Laboratory of Marc Bühler[34]	N/A
M. musculus: Ctrl: R1 stably expressing dCas9	This study	N/A
M. musculus: KD1: R1 stably expressing dCas9 and gRNA for KD1	This study	N/A
M. musculus: KD2: R1 stably expressing dCas9 and gRNA for KD2	This study	N/A
M. musculus: WT7: R1, wild type	This study	N/A

(*Continued on next page*)

Continued		
REAGENT or RESOURCE	SOURCE	IDENTIFIER
M. musculus: WT8: R1, wild type	This study	N/A
M. musculus: pAS1: R1, homozygous insertion of pAS/MAZ into *Meteor*	This study	N/A
M. musculus: pAS2: R1, homozygous insertion of pAS/MAZ into *Meteor*	This study	N/A
M. musculus: WT9: R1, wild type	This study	N/A
M. musculus: WT10: R1, wild type	This study	N/A
M. musculus: pEX1: R1, homozygous insertion of a Hyg/pAS/PGKp into *Meteor*	This study	N/A
M. musculus: pEX2: R1, homozygous insertion of a Hyg/pAS/PGKp into *Meteor*	This study	N/A
M. musculus: pEX3: R1, homozygous insertion of a Hyg/pAS/PGKp into *Meteor*	This study	N/A
Oligonucleotides		
For a list of oligonucleotides used in this study see Table S1	This study	N/A
Recombinant DNA		
pCas9-GFP	Ding et al.[79]	Addgene plasmid #44719
pKLV-U6gRNA	Koike-Yusa et al.[80]	Addgene plasmid #50946
lenti MS2-P65-HSF1_Hygro	Konermann et al.[81]	Addgene plasmid #61426
CSII-U6-gRNA-CBh-3xFLAG-PA-dCas9-P2A-Puro	Deposited by the laboratory of Tohru Kimura	Addgene plasmid #83306
Software and algorithms		
STAR	Dobin et al.[82]	https://github.com/alexdobin/STAR
RSEM	Li and Dewey[83]	https://deweylab.github.io/RSEM/
DEseq2	Love et al.[84]	https://bioconductor.org/packages/release/bioc/html/DESeq2.html
MetaCell	Baran et al.[60]	https://tanaylab.github.io/metacell/
KentUtils	Kent et al.[85]	https://github.com/ENCODE-DCC/kentUtils

RESOURCE AVAILABILITY

Lead contact

Further information and requests for resources and reagents should be directed to and will be fulfilled by the lead contact, Igor Ulitsky (igor.ulitsky@weizmann.ac.il).

Materials availability

This study did not generate new unique reagents.

Data and code availability

- All RNA-seq, 3′RNA-seq, scRNA-seq, 4C, ChIP-seq, and Cut&Run data generated in this study have been deposited at GEO and are publicly available as of the date of publication. Accession numbers are listed in the key resources table. This paper also analyzes existing, publicly available data. These accession numbers for the datasets are listed in the key resources table.
- This paper does not report original code.
- Any additional information required to reanalyze the data reported in this paper is available from the lead contact upon request.

EXPERIMENTAL MODEL AND STUDY PARTICIPANT DETAILS

R1 and 129-C57Bl/6 mESCs were routinely grown on gelatin-coated plates on MEFs, in one of the following media:

Serum-based medium: DMEM (Gibco) containing 15% ES-grade fetal calf serum (Biological Industries), 1X Sodium pyruvate (Gibco), 1X Nonessential amino acids (Gibco), 0.1mM β-mercaptoethanol (Sigma), 100U/ml Penicillin and 0.1 mg/mL Streptomycin

(Biological Industries), and 10 ng/ml LIF (Weizmann Proteomics Unit). Cells were passaged with 0.25% Trypsin (Biological Industries) every 2–3 days.

2i medium: a 1:1 mixture of Neurobasal medium (Gibco) and Knockout DMEM (Gibco), supplemented with 1X B27 (Gibco), 1X N2 (Gibco), 1X Glutamax (Gibco), 1X Sodium pyruvate (Gibco), 1X Nonessential amino acids (Gibco), 0.1mM β-mercaptoethanol (Sigma), 52.5 μg/ml BSA, 100U/ml Penicillin and 0.1 mg/mL Streptomycin (Biological Industries), 1μM PD 0325901 (Axon Medchem), 3μM CHIR 99021 (Axon Medchem), and 10 ng/ml LIF (Weizmann Proteomics Unit). Cells were passaged with 0.25% Trypsin (Biological Industries) every 2–3 days. Trypsin was quenched with serum-based medium, which was removed prior to re-plating.

Primed medium: DMEM/F12 (Sigma) supplemented with 1% Knockout serum replacement (Gibco), 1X B27 (Gibco), 1X N2 (Gibco), 1X Glutamax (Gibco), 1X Sodium pyruvate (Gibco), 1X Nonessential amino acids (Gibco), 0.1mM β-mercaptoethanol (Sigma), 100U/ml Penicillin and 0.1 mg/mL Streptomycin (Biological Industries), 12 ng/ml FGF2 (Peprotech), and 20 ng/ml Activin A (R&D). Cells were passaged with 0.05% Trypsin (Biological Industries) every 3 days. Trypsin was quenched with serum-based medium, which was removed prior to re-plating. 10μm ROCK inhibitor (Axon Medchem) was added to the medium the day before and after each split.

METHOD DETAILS

Generation of promoter KO (pKO) and inversion (pInv) cell lines

To generate *Meteor* promoter KO lines, mESCs were depleted from MEFs by 20 min incubation on gelatin-coated plates and seeded on 6-wells ($5x10^5$ cells/well). mESCs were transfected with pCas9-GFP and two pKLV-U6gRNA plasmids containing gRNAs targeting the two sides of the *Meteor* TSS (see Table S1). Transfections were carried out using Xfect mESC Transfection Reagent (Takara Bio) according to manufacturer's instructions. MEFs were added 3h post-transfection. 0.8 μg/μL Puromycin was added to the medium 24h after transfection for selection. Six days after transfection, mESCs were seeded at a very low density on a 10cm plate. Colonies were picked, expanded, and the genomic deletion was verified using PCR and single molecule FISH (see Figures S1B–S1C and Table S1). Lack of *Meteor* expression was verified by qRT-PCR and RNA-seq. Clones that underwent a similar process but did not exhibit the genomic deletion were expanded alongside and used as WT controls.

Generation of polyA insertion (pAS) cell lines

Meteor polyA insertion mESCs were generated by transfection with a pKLV-U6gRNA plasmid containing gRNA 2 that was used for generating *Meteor* pKO lines (see Table S1), pCas9-GFP, and a ssODN (200nt) containing two homology arms (50nt each), a short poly(A) site (49nt), and two MAZ sites.[86] Colonies were picked, expanded, and the poly(A)/MAZ insertion was confirmed by PCR amplifications and sequencing (Table S1). Clones without an insertion were expanded alongside and used as WT controls.

Generation of PGK promoter exchange (pEX) cell lines

The PGK promoter knock in vector (pBlueScript-KS+ vector (Stratagene)) was generated by insertion of *Meteor* 5′ homology arm (*Meteor* promoter, 985 bp in length, mm9 coordinates chr9:118,315,278-118,316,262) and 3′ homology arm (*Meteor* first exon, 362 bp, mm9 coordinates chr9:118,314,889-118,315,250) upstream of a Hygromycin resistance gene and a pAS (taken from Addgene plasmid #61426) and downstream of a PGK promoter (taken from pKLV-U6gRNA), respectively (see Figure 1A).[87] The targeting vector was co-transfected with pCas9-GFP and pKLV-U6gRNA plasmids containing gRNA pEX (see Table S1) which targets immediately upstream of *Meteor* TSS. 0.8 μg/μL Puromycin and 4 μg/μL Hygromycin were added to the medium 24h after transfection. Six days after transfection, mESCs were seeded at a very low density on a 10cm plate. Colonies were picked, expanded, and the Hygromycin resistance and PGK insertion was verified using PCR (Table S1). Clones without an insertion were expanded alongside and used as WT controls.

Generation of dCas9-KD cell lines

Viruses were produced by transfecting HEK293T cells with a 1:0.65:0.35:0.25 ratio of CSII-U6-gRNA-CBh-3xFLAG-PA-dCas9-P2A-Puro, pMDL, pVSVG, and pRev plasmids, respectively, using PEI transfection.[88] Medium was collected 48h after transfection, filtered, and kept at −80°C.

These viruses were used to create mESCs stably expressing dCas9: mESCs were depleted from MEFs by 20 min incubation on gelatin-coated plates, and $6x10^5$ cells were incubated in 1.5mL of virus-containing medium for 30 min at 37°C, and then seeded on two 6-wells. 0.8 μg/μL Puromycin was added to the medium 24h after transfection. Surviving colonies were seeded at a very low density on a 10cm plate. Colonies were picked, expanded, and the presence and expression of dCas9 was assayed by PCR and Western Blot.

Meteor dCas9-KD mESCs were created by infecting the dCas9-expressing mESCs with viruses prepared as described above from pKLV-U6gRNA plasmids containing gRNAs targeting the vicinity of the *Meteor* TSS (see Table S1). 48h post-infection, mESCs were sorted for BFP expression using FACSAria II (BD Biosciences), and screened for *Meteor* KD using qRT-PCR and RNA-seq.

EB differentiation

mESCs were depleted from MEFs by 20 min incubation on gelatin-coated plates, and seeded at 500cells/27μL drop in differentiation medium (serum-based mESC medium without LIF), on the lids of 10cm plates with PBS. On d2 drops were collected, combined, and

transferred to non-adherent 10cm petri dishes in differentiation medium. On d7 individual EBs were transferred to separate gelatin-coated 24-wells and grown in differentiation medium for five additional days. EBs were screened for beating foci at day 9 and day 12 of differentiation. RNA expression throughout the differentiation was assayed using 3′ mRNA-Seq or qRT-PCR (see Table S1 for primer sequences).

Neuronal differentiation

Neuronal differentiation was based on a protocol taken from.[89] mESCs were grown for two passages in serum-based medium on MEF-free, gelatin-coated plates. Cells were then seeded on gelatin-coated plates ($2x10^5$ cells/6-well) in neuronal differentiation medium: 1:1 mixture of DMEM/F12 (Sigma) and Neurobasal medium (Gibco), supplemented with 0.5X B27 (Gibco), 0.5X N2 (Gibco), 1X Glutamax (Gibco), 0.1mM β-mercaptoethanol (Sigma), 25 μg/ml BSA, and 100U/ml Penicillin and 0.1 mg/mL Streptomycin (Biological Industries). After four days, the cells were dissociated with 0.05% Trypsin (Biological Industries) and re-plated ($3.5x10^5$/6-well) on Poly-D-Lysine (Sigma) and Laminin (Life)-coated plates, in neuronal differentiation medium also containing 20 ng/ml FGF2 (Peprotech). FGF2 was removed after 24hr and the cells were grown for an additional three days.

For stainings,[65] cells were fixed in 4% paraformaldehyde for 15 min, and incubated in blocking buffer (5% donkey serum, 2% BSA, and 0.1% Triton X-100 in PBS). Primary antibodies (mouse anti-Nestin (Abcam ab6142) or rabbit anti-Beta III Tubulin (Tuj1, Abcam ab18207)) were diluted in permeabilization buffer (same as above, without Triton X-100) and incubated with the cells at 4°C overnight. Secondary antibodies (donkey anti-mouse Alexa 594 (Molecular Probes A21203) or goat anti-rabbit Alexa 594 (Abcam ab150080)) were diluted in permeabilization buffer and incubated with fixed cells for 2h at RT. Imaging was done using the EVOS FL Cell Imaging System.

RNA sequencing

0.5–1μg total RNA was used to prepare RNA-seq libraries using either the SENSE mRNA-Seq Library Prep Kit V2 (Lexogen) or the QuantSeq 3′ mRNA-Seq Library Prep Kit for Illumina (FWD) (Lexogen), according to the manufacturer's protocols, and sequenced on either a NextSeq 500 or Novaseq 6000 machine. Reads were mapped to the mouse genome (mm9) using STAR.[82] Expression levels were quantified using RSEM,[83] and differential expression analysis was performed using DESeq2.[84] For 3′ RNA-seq, RSEM was run on a gene annotation GTF file where the last exon of each gene was extended by 2Kb to the 3′ direction if no other gene was found on the same strand within that distance, to ensure that reads falling outside the annotated genes were assigned correctly.

For scRNA-seq, cells were sorted into 384-well plates containing 2nM barcodes and lysis buffer. After MARS-seq barcoding and library preparation[90] the libraries were sequenced on a NextSeq 500 machine. UMI matrices were generated, summarizing the expression levels of all genes across all WT and *Meteor* pKO cells,[91,92] and metacells were constructed and analyzed using the MetaCell package.[60]

Chromatin immunoprecipitation (ChIP)

ChIP was performed[93] by crosslinking $1x10^7$ cells in 1% formaldehyde for 10 min at RT, and the reaction was quenched by addition of 125mM glycine and 5 min incubation at RT. Cells were centrifuged 5 min at 2000xg, 4°C, washed three times in PBS containing protease inhibitors (PI), and lysed in 1mL lysis buffer (5mM PIPES pH 8.0, 85mM KCl, 1% Igepal, and 1X PI) for 15 min on ice. Cells were centrifuged 5 min at 250Xg, 4°C, supernatant was discarded, and nuclei were lysed by incubation in nuclei lysis buffer (50mM Tris-HCl pH 8.1, 10mM EDTA pH 8.0, 1% SDS, and 1X PI) for 30 min on ice, followed by flash freezing in liquid nitrogen and re-thawing. Pellets were sonicated using a Bioruptor for either 12 (mESCs) or 15 (NPCs) cycles in high setting, 30 s ON, 30 s OFF, centrifuged 10 min at 14,000rpm, 4°C, and supernatant was transferred to a new tube and diluted ×10 in IP dilution buffer (50mM Tris-HCl pH 7.4, 150mM NaCl, 1% Igepal, 0.25% Deoxycholic acid, 1mM EDTA pH 8.0, and 1X PI). 50μL protein A/G magnetic beads (GenScript, Cat #L00277) per IP were washed twice in binding/washing buffer (0.5% BSA and 0.5% Tween 20 in PBS), resuspended in 1 mL binding/washing buffer with either anti-H3K27ac (D5E4) antibody (Cell Signaling #8173) or anti-CTCF (D31H2) antibody (Cell Signaling, #3418), and incubated >1h at RT with rotation. Beads were washed with 1.5mL binding/washing buffer, and ∼60μg chromatin per IP was added and incubated overnight at 4°C rotation. IPs were washed on ice six times with RIPA buffer (10mM Tris-HCl pH 8.0, 140mM NaCl, 1mM EDTA pH 8.0, 1% Triton X-100, 0.1% SDS, 0.1% Deoxycholic acid; first wash also contained 1X PI), twice with RIPA-500 buffer (same, except with 500mM NaCl), twice with LiCl wash buffer (10mM Tris-HCl pH 8.0, 1mM EDTA pH 8.0, 250mM LiCl, 0.5% NP-40, and 0.5% Deoxycholic acid), once with TE (10mM Tris-HCl pH 8.0 and 1mM EDTA pH 8.0), and then resuspended in 50μL of direct elution buffer (10mM Tris-HCl pH 8.0, 5mM EDTA pH 8.0, 300mM NaCl, and 0.5% SDS). Decrosslinking was done by incubating with 1μg RNAse for 30 min at 37°C, followed by addition of 20μg Glycogen and 50μg proteinase K and incubation for 2h at 37°C and overnight at 65°C. DNA was cleaned with 2.3x AMPure XP breads and eluted in 60μL of 10mM Tris-HCl pH 8.0.

Library preparation was done by end repair, A-tailing, and adapter ligation,[94] followed by sequencing on either a NextSeq 500 or NovaSeq 6000 instrument.

Cut&Run

For Cut&Run analysis,[95] $2x10^5$ cells were pelleted 3 min at 600xg, washed twice in 1.5mL Wash buffer (20mM Hepes-Naoh pH 7.5, 150mM NaCl, 0.5mM Spermidine, and 1X protease inhibitors), and resuspended in 300μL Wash buffer. 10μL of BioMag Plus

Concanavalin A beads (#BP531, WeisScientific) were washed twice in Binding buffer (20mM Hepes-KOH pH 7.9, 10mM KCl, 1mM CaCl2, and 40mM $MnCl_2$) and added to the cells. Cell-bead mixture was rotated 5–10 min at RT, magnetized, resuspended in 150μL Antibody buffer (Wash buffer with 0.15% Digitonin, 2mM EDTA, and 1.5μL of either H3K27me3 antibody (C36B11, Cell Signaling #9733) or H3K4me3 antibody (C42D8, Cell Signaling #9751), and incubated overnight at 4°C.

Cells were washed twice in Dig-Wash buffer (Wash buffer also containing 0.15% Digitonin), resuspended in 150μL Dig-Wash buffer containing 350 ng/ml pA-MNAse (Weizmann Proteomics Unit), and rotated 1h at 4°C. Cells were then washed twice with Dig-Wash buffer, resuspended in 100μL Dig-Wash buffer, and placed in ice water for a few minutes. MNAse was activated by adding 2μL of 100mM $CaCl_2$ and incubating 30 min on ice. Reaction was stopped by adding 100μL 2X STOP buffer (340mM NaCl, 20mM EDTA, 4mM EGTA, 0.15% Digitonin, 100 μg/ml RNAse A, and 50 μg/ml glycogen). Chromatin fragments were released by incubating 30 min at 37°C, transferring the supernatant to new tubes, and incubating 1h at 50°C with 1μL 20% SDS and 2.5μL 20 mg/ml Proteinase K. DNA was isolated using phenol-chloroform extraction. Library construction was done by end repair, A-tailing, adaptor ligation, and amplification[95,96] and libraries were sequenced on either a NextSeq 500 or NovaSeq 6000 instrument.

Targeted chromosome conformation capture (4C)

mESC cultures were depleted from MEFs by 20 min incubation on gelatin-coated plates. 3C[92] was carried out on $5x10^6$ cells, with the following slight modification from the protocol.[42,97] permeabilization buffer constitution was 10 mM Tris-HCl pH 8, 10 mM NaCl, 0.5% NP-40, supplemented with protease inhibitors. For a list of primers used for the 4C analysis, see Table S1. Libraries were sequenced on either a NextSeq 500 or NovaSeq 6000 instrument, and analyzed using the UMI-4C package.[42]

QUANTIFICATION AND STATISTICAL ANALYSIS

Statistical analyses

The statistical analyses and software used are indicated in the **Method Details** section. Statistical tests used, including replicate numbers, are indicated in the figure legends, and all computed p values are indicated in the figures.

Cut&Run data analysis

H3K27me3 signal was quantified using the bigWigAverageOverBed tool of the kentUtils package as mean signal of three repeats at the following regions: the *Meteor* gene body (mm9 coordinates chr9:118,306,226–118,315,298), a region encompassing the *Meteor* locus and downstream enhancer (mm9 coordinates chr9:118,286,700–118,314,400), and an H3K27me3-rich control region at the HoxB locus (mm9 coordinates chr11:96,149,799–96,216,130). Signal was normalized to the WT1 cell line and to a control region near the *Ppib* gene (mm9 coordinates chr9:65,914,278–65,932,710).

Cell Reports, Volume *42*

Supplemental information

Complex regulation of *Eomes* levels mediated through distinct functional features of the *Meteor* long non-coding RNA locus

Noa Gil, Rotem Ben-Tov Perry, Zohar Mukamel, Alex Tuck, Marc Bühler, and Igor Ulitsky

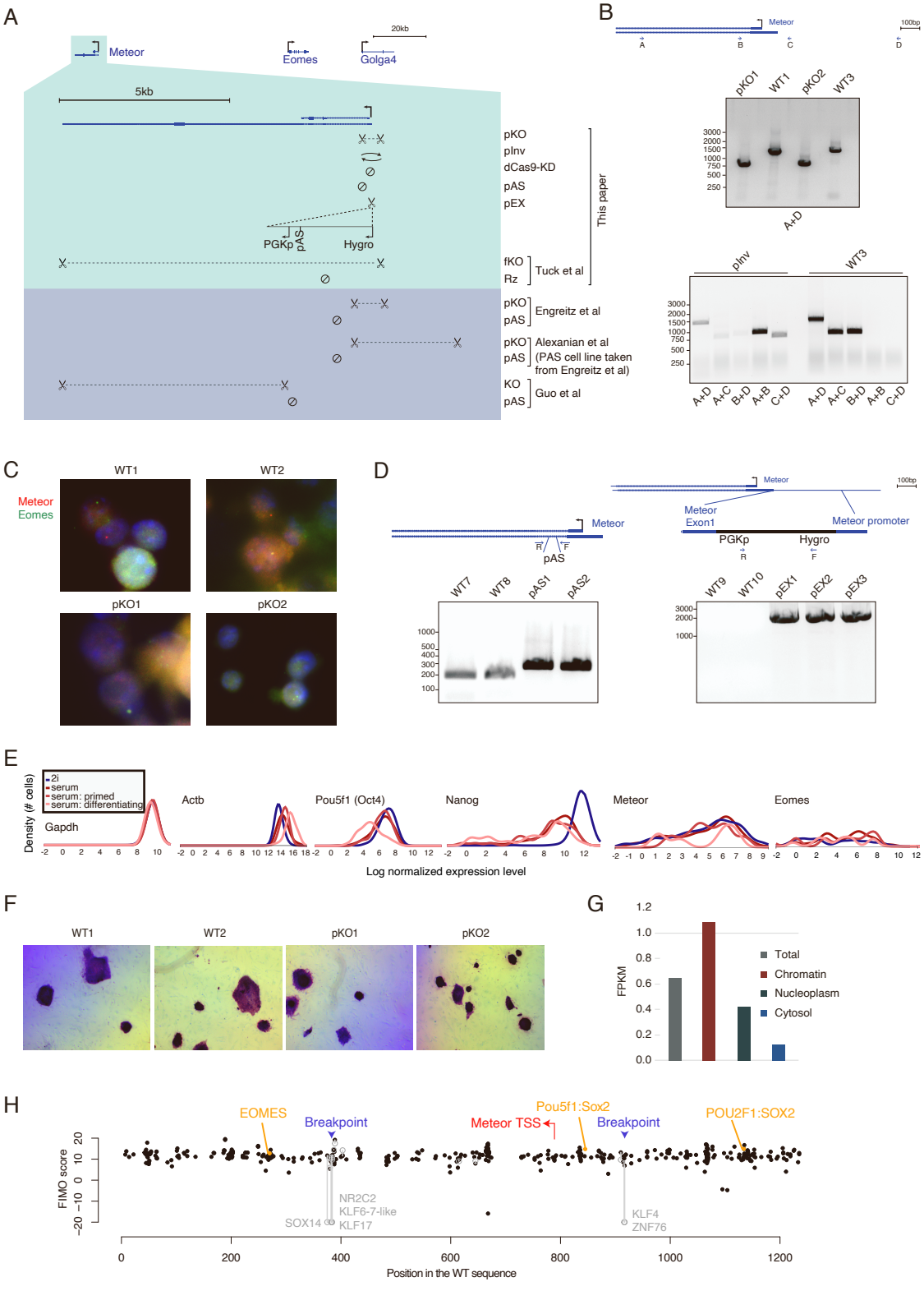
A
Meteor
Eomes
Golga4
20kb
5kb
PGKp
pAS
Hygro
pKO
pInv
dCas9-KD
pAS
pEX
fKO
Rz
Tuck et al
This paper
pKO
pAS
Engreitz et al
pKO
pAS
Alexanian et al
(PAS cell line taken
from Engreitz et al)
KO
pAS
Guo et al
B
Meteor
100bp
A
B
C
D
pKO1
WT1
pKO2
WT3
3000
2000
1500
1000
750
500
250
A+D
pInv
WT3
A+D
A+C
B+D
A+B
C+D
C
WT1
WT2
Meteor
Eomes
pKO1
pKO2
D
Meteor
100bp
Meteor
Exon1
Meteor promoter
Meteor
PGKp
Hygro
pAS
R
F
WT7
WT8
pAS1
pAS2
1000
500
400
300
200
100
WT9
WT10
pEX1
pEX2
pEX3
3000
2000
1000
E
2i
serum
serum: primed
serum: differentiating
Density (# cells)
Gapdh
Actb
Pou5f1 (Oct4)
Nanog
Meteor
Eomes
Log normalized expression level
F
WT1
WT2
pKO1
pKO2
G
FPKM
1.2
1.0
0.8
0.6
0.4
0.2
0.0
Total
Chromatin
Nucleoplasm
Cytosol
H
EOMES
Breakpoint
Meteor TSS
Pou5f1:Sox2
Breakpoint
POU2F1:SOX2
FIMO score
20
10
0
−10
−20
NR2C2
KLF6-7-like
KLF17
SOX14
KLF4
ZNF76
0
200
400
600
800
1000
1200
Position in the WT sequence

Figure S1. Perturbations to the *Meteor* locus. Related to Figure 1.

A. (Top) same as Figure 1A, and (bottom) additional genomic perturbations described in the indicated papers [S1–4] for deleting regions in the *Meteor* locus (KO) or introducing polyadenylation sites (pAS). **B.** Schematic locations and directionalities of the primers used to probe genomic deletions in the *Meteor* locus (top), and the resulting PCR products (bottom). PCR was performed on the indicated cell lines using the primers indicated below the blots (see **Method Details** and **Table S1**). PCR using primers B and C was performed on DNA pre-amplified with primers A and D. **C.** Single molecule FISH using probes against *Meteor* (red) and *Eomes* (green) as well as DAPI staining (blue) in WT and *Meteor* pKO cells grown in 2i conditions, imaged using 100X objectives. No *Meteor* signal was detected in the pKO lines. **D**. Same as (B), for genotyping pAS insertions (left) and pEX clones (right). PCR was performed on the indicated cell lines using the primers listed in **Table S1**. **E.** Density plots of expression levels of the indicated genes in the indicated cell populations visualized through the ESpresso database [S5]. **F.** AP staining for the pluripotent state of pKO clones. **G.** Expression levels of *Meteor* in the indicated compartment of mESCs. Data taken from GEO dataset GSE99366. **H.** Predicted binding scores for TF binding sites (TFBS) defined in the JASPAR database [S6] in the WT and pInv sequence surrounding the *Meteor* TSS. The position of the TSS and the positions of the inversion breakpoints are shown by vertical lines. For each TFBS, the position with the highest score in the WT sequence is denoted by a black dot and shown at the position of the top-scoring hit in the WT sequence. For TFBSs for which the score in the inverted sequence is different, a gray point indicates the highest score in the inverted sequence, and the gray lines connect the scores in the WT and the inverted sequences. Scores below –20 were set to –20. Names of TFBSs for which the scores were below –20 in the inverted sequence are shown in gray. Scores for the pluripotency TFs and for EOMES are denoted in orange.

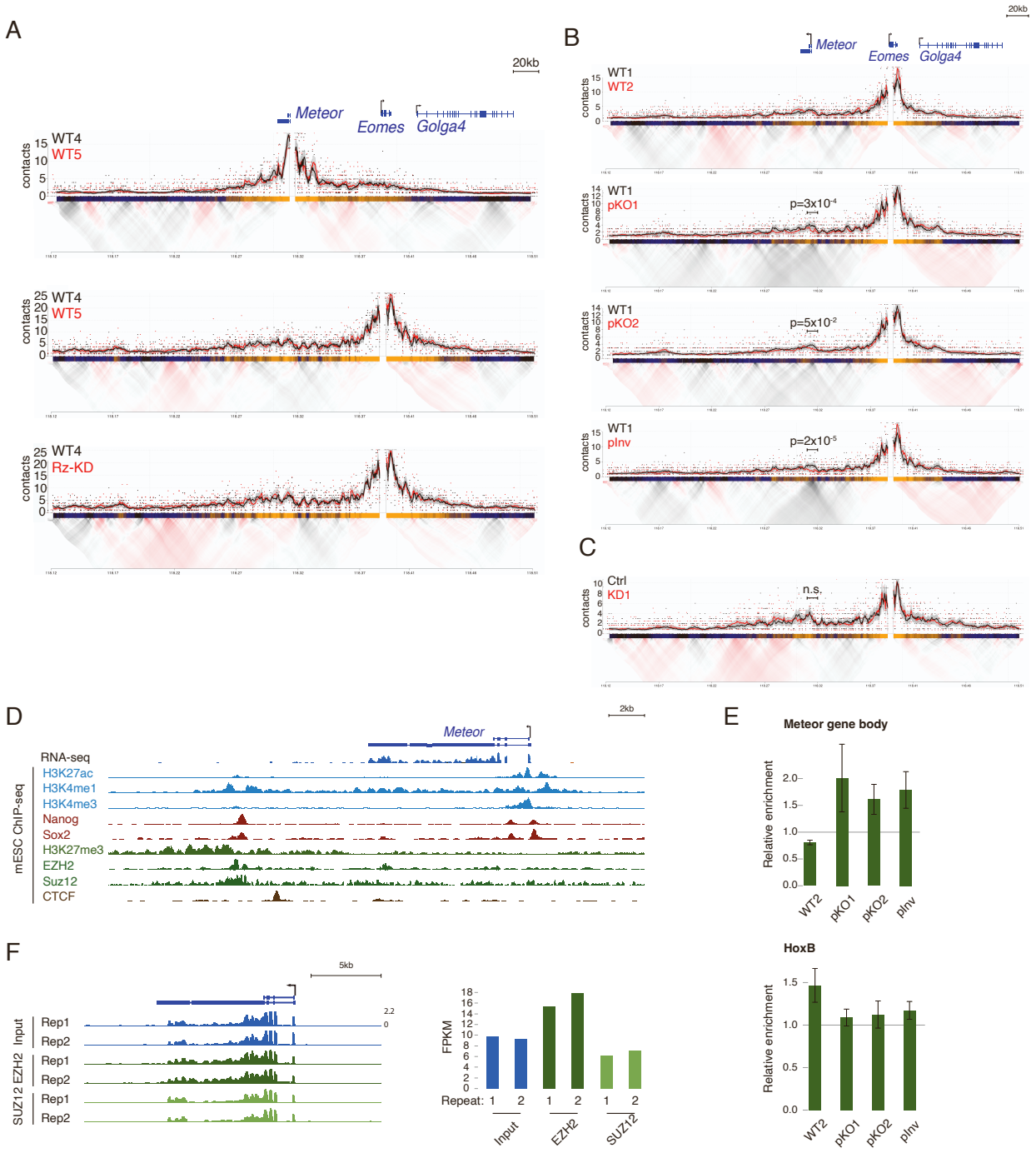

Figure S2. *Meteor* depletion induces chromatin changes in mESCs. Related to Figure 2.

A. 4C analysis in the indicated mESC lines using either the *Meteor* or *Eomes* promoters as viewpoints. Domainograms showing mean contact per fragment end for a series of window sizes are placed below smoothed trend lines and raw counts of the contact profiles. **B.** Same as (A), for *Meteor* pKO and pInv mESCs, using the *Eomes* promoter as the viewpoint. **C.** Same as (A), for *Meteor* KD mESCs, using the *Eomes* promoter as the viewpoint. **D.** Genome browser image of the *Meteor* locus. Shown are representative transcript models; RNA-seq tracks where orange denotes transcription on the plus strand

and blue denotes transcription on the minus strand; and mESC ChIP-seq tracks. **E.** Quantification of H3K27me3 Cut&Run levels in mESC lines grown in serum-free 2i/LIF conditions. Shown are H3K27me3 levels around the *Meteor* gene body, and at a control region around the *HoxB* locus. Signal was normalized to WT1 and to a H3K27me3-rich region near the *Ppib* gene (see **STAR Methods**). Bars represent standard errors; n=3. **F.** (Left) Genome browser shot of the *Meteor* locus, showing RNA immunoprecipitation (RIP) data of WT mESCs taken from [S7]. All tracks are normalized to the same scale. (Right) RSEM quantification of signal from the *Meteor* region in the same samples.

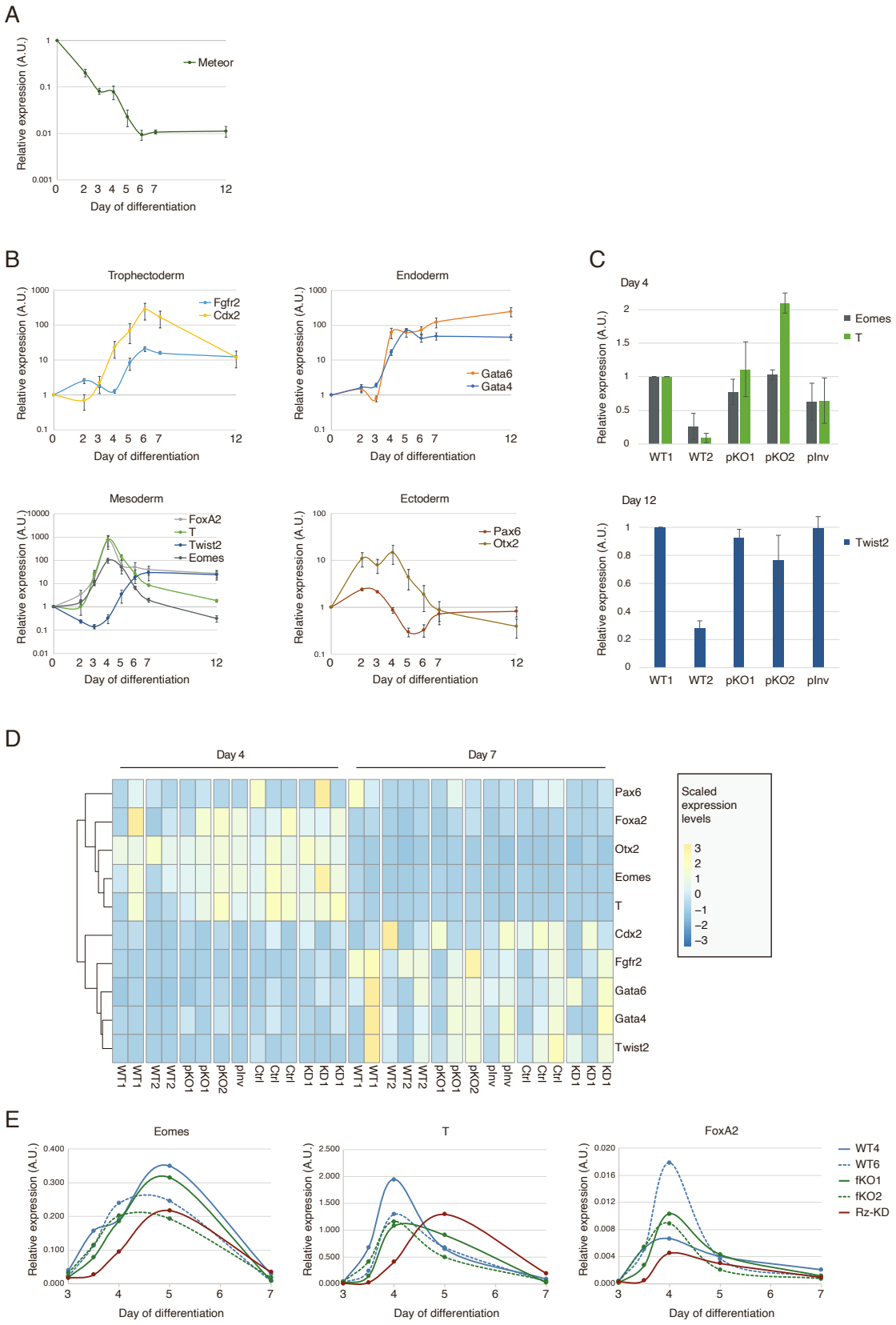
A
Meteor
Relative expression (A.U.)
Day of differentiation
B
Trophectoderm
Fgfr2
Cdx2
Endoderm
Gata6
Gata4
Mesoderm
FoxA2
T
Twist2
Eomes
Ectoderm
Pax6
Otx2
C
Day 4
Eomes
T
WT1
WT2
pKO1
pKO2
pInv
Day 12
Twist2
D
Day 4
Day 7
Pax6
Foxa2
Otx2
Eomes
T
Cdx2
Fgfr2
Gata6
Gata4
Twist2
Scaled expression levels
E
Eomes
T
FoxA2
WT4
WT6
fKO1
fKO2
Rz-KD

Figure S3. *Meteor* repression does not alter the cardiac mesoderm differentiation potential of mESCs. Related to Figure 3.

A. qRT-PCR quantifications of *Meteor* levels throughout EB differentiation. Levels were normalized to Sdha and to expression in mESCs (day 0). Bars represent standard errors; n=4. **B.** Same as (A), for the indicated markers of the different germ layers. **C.** qRT-PCR quantifications of the indicated mesoderm markers at day 4 (top) or day 12 (bottom) of EB differentiation of the indicated cell lines. Levels were normalized to Sdha. Bars represent standard errors; n=2. **D.** Heatmap of the scaled FPKM expression levels of the indicated genes in 3' RNA-seq data from the indicated day of EB differentiation. Each gene was scaled separately to mean 0 and standard deviation 1 across all the samples. **E.** qRT-PCR quantifications of the indicated markers at several time points throughout EB differentiation of the indicated cell lines. Levels were normalized to Sdha. n=2.

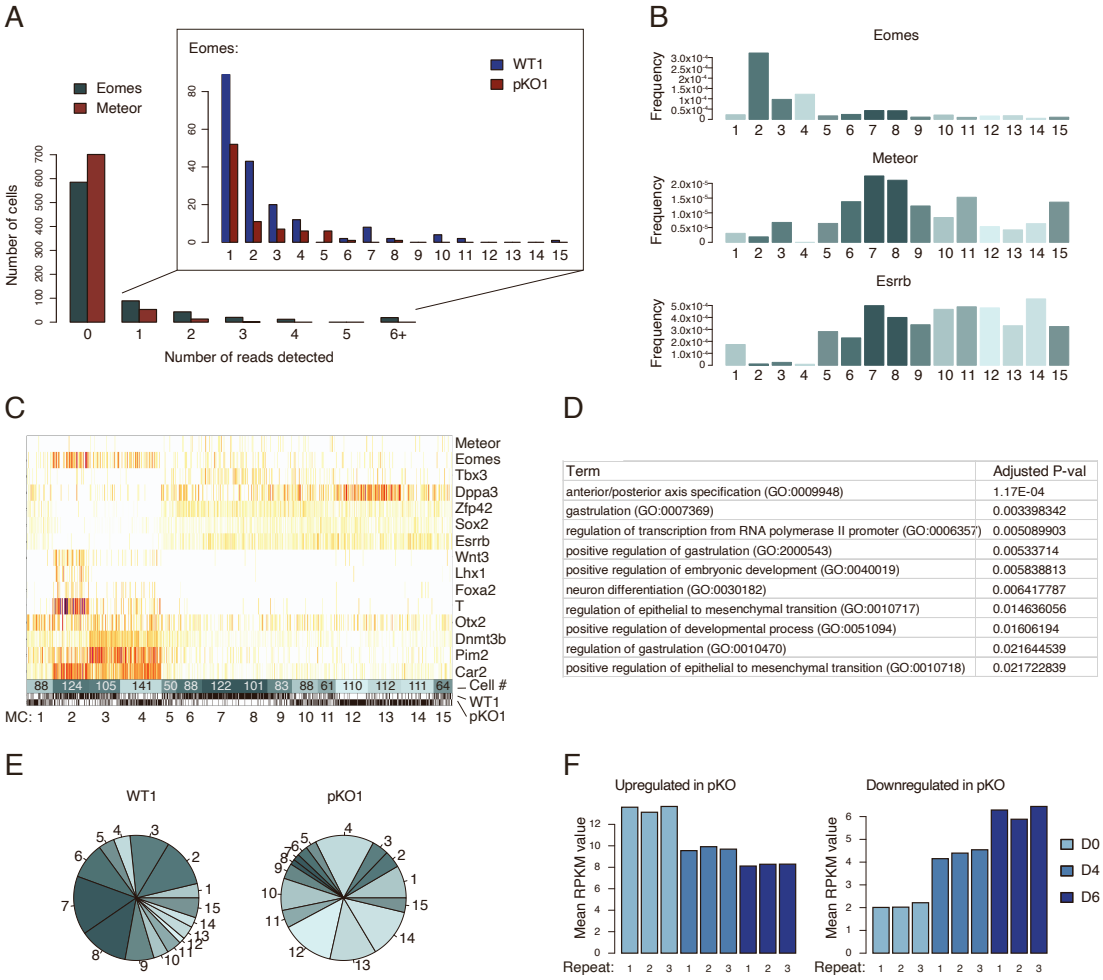

Figure S4. Single-cell RNA-seq of WT and *Meteor* pKO cells. Related to Figure 4.

A. Distribution of the number of unique reads per cell originating from the indicated transcript, for scRNA-seq of WT mESCs. Inset: same, for *Eomes* only, separately for WT and *Meteor* pKO cells, and showing only cells in which ≥1 *Eomes* reads were detected. **B.** Frequency of the indicated genes in each of the metacells (MCs). Color was assigned to each MC according to the ratio of WT and pKO cells that comprise it, with darker shades representing MCs comprised mostly of WT cells and lighter shades representing MCs comprised mostly of pKO cells. **C.** Heatmap showing enrichment values of the indicated key genes in individual cells (columns), grouped into MCs. Below: color assignments as in (B), overlayed with the number of cells in each MC; indication of the mESC line from which the cells originate; and MC number. **D.** GO terms associated with the 100 genes most highly correlated with *Eomes* in the scRNA-seq data. GO terms identified using Enrichr. **E.** Number of cells occupying the indicated MCs, separately for WT and pKO cells. Color assignments as in (B). **F.** Mean expression values of all the differentially regulated genes (FC ≥ 1.5 and padj < 0.05 in bulk RNA-seq of both *Meteor* pKO1 and pKO2), separately for upregulated (left) and downregulated (right) genes, in different timepoints of a dataset of control mESCs undergoing neural differentiation taken from [S8]. D0: pluripotent mESCs; D4: multipotent progenitors; D6: early neural progenitors.

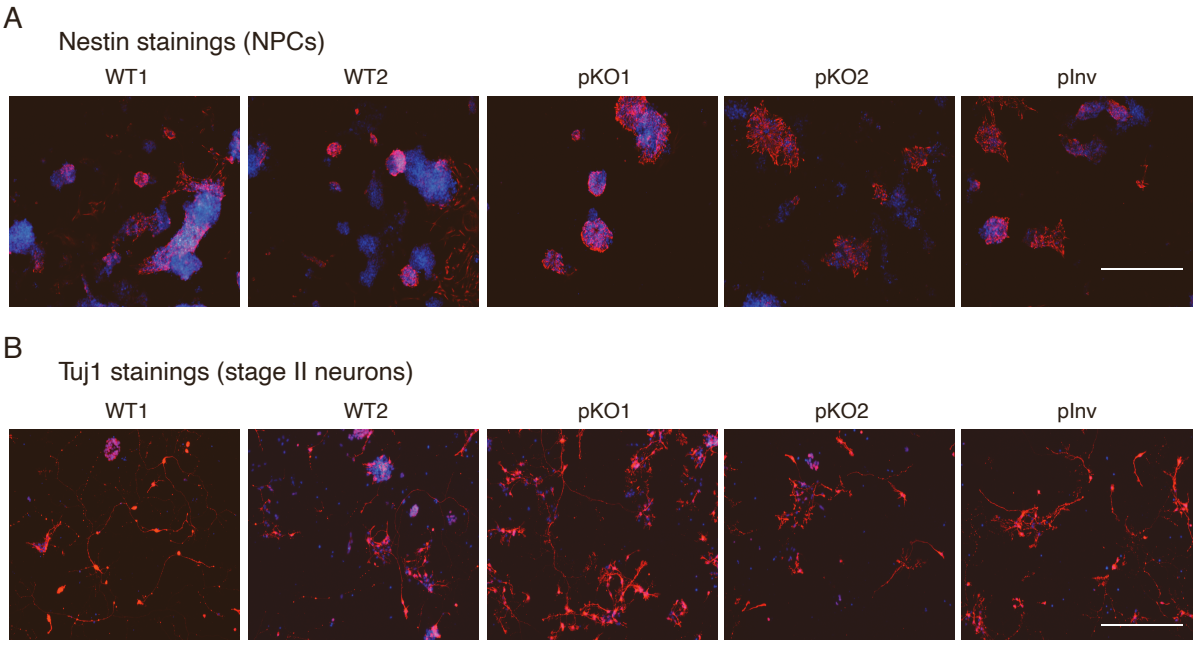

Figure S5. Neuronal differentiation of WT and *Meteor*-depleted cell lines. Related to Figure 5.

A. Nestin (red) stainings in NPCs derived from the indicated cell lines. Blue shows DAPI-colored nuclei. Scale bar = 400 µm. **B.** Same as (A), for Tuj1 (red) stainings in stage II neurons.

Table S1. Sequences of oligonucleotide used in this study, related to STAR Methods.

Purpose	Name	Sequence
4C of *Meteor* promoter	Upstream primer	tggggtccgaggcagagaacgcga
	Downstream primer	aatgatacggcgaccaccgagatctacactctttccctacacga cgctcttccgatctagagacagaagaagtcactatggc
4C of *Meteor* promoter in pKO mESCs	Upstream primer	tctaccagaagtgctaaagggatg
	Downstream primer	aatgatacggcgaccaccgagatctacactctttccctacacga cgctcttccgatctgtaatctataaagtgcttgcctata
4C of *Eomes* promoter	Upstream primer	ctacctgtgcaaccggcccctatg
	Downstream primer	aatgatacggcgaccaccgagatctacactctttccctacacga cgctcttccgatcttcaaattccaccggcaccaaactg
Meteor pKO	gRNA 1	aaaagctcggtagtaagagg
	gRNA 2	gccgtgaacattattcgggg
Meteor pKO genotyping	Primer A	aaattcgaggctggcactctgct
	Primer B	tgggcagataccaaccctct
	Primer C	agatgcccacagccaaaact
	Primer D	ggccaatcttgagtcttccgca
Meteor dCas9-KD	gRNA for KD1	gagctcacggacatgagg
	gRNA for KD2	gtccgaggcagagaacgcga
pAS cassette		tttgggggtcctaggcaggggcttccagaggtgcttggcactgct tggcacccctcccccgactcgattgtacgtgaagctccccctcc ccccgatcaagcacacaaaaaaccaacacacagatctaatgaa aataaagatcttttattcgggcagtaagtgtctcagctccattca gactgctgaccttggcatgggc
Meteor pAS genotyping	Forward primer	atccattgctcattcatttgca
	Reverse primer	tgggttatcgacagggaagt
Meteor PGK pEX cloning	*Meteor* Insertion F	gtaatacgactcactatagggcgaattggttggatttctgaccct cctg
	Meteor Insertion R	tgcttatgccatagtgacttcttctgtctcgcccgccgcgcgcttc g
	Hygromycin F	gagctcggttcccaggcttgggcatgaaaaagcctgaactcacc
	Hygromycin R	tccttcgcgttctctgcctcggccatagagcccaccgcat
	PGK F	ccgaggcagagaacgcgaaggaaggggtaggggagg
	PGK R	tagtgacttcttctgtctcgaaaggcccggagatgagg
Meteor PGK pEX	gRNA pEX	caagcctgggaaccgagctc
Meteor pEX genotyping	Forward primer	atacgaggtcgccaacatct
	Reverse primer	cttgggaaaagcgcctcccc
qRT-PCR of *Meteor*	Forward primer	aggactggcctgctagagaa
	Reverse primer	agtcagacagagcatccatcc

qRT-PCR of *Eomes*	Forward primer	tgtgacggcctaccaaaaca
	Reverse primer	tctgatgggatgaatcgtagttgt
qRT-PCR of *Fgfr2*	Forward primer	aaagaccacaaatgggcgac
	Reverse primer	ccacattaacaccccgaagga
qRT-PCR of *Cdx2*	Forward primer	gcggctggagctggagaaggagtt
	Reverse primer	cggcggctgtggaggctgttgt
qRT-PCR of *Gata4*	Forward primer	agctccatgtcccagacattc
	Reverse primer	agatgcatagccttgtgggg
qRT-PCR of *Gata6*	Forward primer	gacggcaccggtcattacc
	Reverse primer	acagttggcacaggacagtcc
qRT-PCR of *FoxA2*	Forward primer	ggagcccgagggctactct
	Reverse primer	gagcccgcgctcatgtt
qRT-PCR of *T*	Forward primer	gctctaaggaaccaccggtcatc
	Reverse primer	atgggactgcagcatggacag
qRT-PCR of *Twist2*	Forward primer	gtctcagctacgccttctcc
	Reverse primer	caggtgggtcctggcttg
qRT-PCR of *Pax6*	Forward primer	gggaccacttcaacaggact
	Reverse primer	cgaggccagtactgagacat
qRT-PCR of *Otx2*	Forward primer	aagacccggtacccagacatc
	Reverse primer	ttggcggcacttagctcttc
qRT-PCR of *Sdha*	Forward primer	gctcctgcctctgtggttga
	Reverse primer	agcaacaccgatgagcctg
qRT-PCR of *Ppib*	Forward primer	tgatccagggtggagacttc
	Reverse primer	attggtgtctttgcctgcat

References

[S1] Tuck AC, Natarajan KN, Rice GM, Borawski J, Mohn F, Rankova A, et al. Distinctive features of lincRNA gene expression suggest widespread RNA-independent functions. Life Sci Alliance 2018;1:e201800124.

[S2] Engreitz JM, Haines JE, Perez EM, Munson G, Chen J, Kane M, et al. Local regulation of gene expression by lncRNA promoters, transcription and splicing. Nature 2016;539:452–5.

[S3] Alexanian M, Maric D, Jenkinson SP, Mina M, Friedman CE, Ting C-C, et al. A transcribed enhancer dictates mesendoderm specification in pluripotency. Nat Commun 2017;8:1806.

[S4] Guo X, Xu Y, Wang Z, Wu Y, Chen J, Wang G, et al. A Linc1405/Eomes Complex Promotes Cardiac Mesoderm Specification and Cardiogenesis. Cell Stem Cell 2018;22:893–908.e6.

[S5] Kolodziejczyk AA, Kim JK, Tsang JCH, Ilicic T, Henriksson J, Natarajan KN, et al. Single Cell RNA-Sequencing of Pluripotent States Unlocks Modular Transcriptional Variation. Cell Stem Cell 2015;17:471–85.

[S6] Castro-Mondragon JA, Riudavets-Puig R, Rauluseviciute I, Berhanu Lemma R, Turchi L, Blanc-Mathieu R, et al. JASPAR 2022: the 9th release of the open-access database of transcription factor binding profiles. Nucleic Acids Res 2022;50:D165–73.

[S7] Garland W, Comet I, Wu M, Radzisheuskaya A, Rib L, Vitting-Seerup K, et al. A Functional Link between Nuclear RNA Decay and Transcriptional Control Mediated by the Polycomb Repressive Complex 2. Cell Rep 2019;29:1800–11.e6.

[S8] Stryjewska A, Dries R, Pieters T, Verstappen G, Conidi A, Coddens K, et al. Zeb2 Regulates Cell Fate at the Exit from Epiblast State in Mouse Embryonic Stem Cells. Stem Cells 2017;35:611–25.